

**Fasting-Induced Intestinal Apoptosis is Mediated by Inducible Nitric Oxide Synthase and Interferon- $\gamma$  in Rat**

**Junta Ito, Hiroyuki Uchida, Takayuki Yokote, Kazuo Ohtake, and Jun Kobayashi**

*Division of Pathophysiology, Department of Clinical Dietetics and Human Nutrition, Faculty of*

*Pharmaceutical Science, Josai University, Saitama, Japan*

Running head: Fasting-induced apoptosis mediated by iNOS and IFN- $\gamma$

Corresponding author: Jun Kobayashi

Fax: +81 49 271 7209.

E-mail address: junkoba@josai.ac.jp

## **ABSTRACT**

Nitric oxide (NO) is associated with intestinal apoptosis in health and disease. This study aimed to investigate the role of intestinal NO in the regulation of apoptosis during fasting in rats. Male Wistar rats were divided into two groups and subcutaneously injected with saline (SA) or aminoguanidine (AG), followed by fasting for 24, 48, 60 and 72 h. At each time point, the jejunum was subjected to histological evaluation for enterocyte apoptosis using histomorphometric assessment and TUNEL analysis. We performed immunohistochemistry for inducible NO synthase (iNOS) expression in the jejunum and measured tissue nitrite levels using HPLC and 8-hydroxydeoxyguanosine adduct using ELISA, indicative of endogenous NO production and reactive oxygen species (ROS) production, respectively. Jejunal transcriptional levels of iNOS, neuronal NO synthase (nNOS) and interferon- $\gamma$  (IFN- $\gamma$ ) were also determined using RT-PCR. Fasting caused significant jejunal mucosal atrophy due to increased apoptosis, and attenuated cell proliferation with increased iNOS transcription, its protein expression in intestinal epithelial cells (IEC), and jejunal nitrite levels. However, AG treatment histologically reduced apoptosis with inhibition of fasting-induced iNOS transcription, protein expression, and nitrite production. We also observed fasting-induced ROS production and subsequent IFN- $\gamma$  transcription, which were all inhibited by AG treatment. Furthermore, we observed reduced transcriptional levels of nNOS, known to suppress iNOS activation physiologically. These results suggest that fasting-induced iNOS activation in IEC may induce apoptosis mediators such as IFN- $\gamma$  via a ROS-mediated mechanism, and also a possible role of nNOS in the regulation of iNOS activity in fasting-induced apoptosis.

**Keywords:** Fasting, Apoptosis, Nitric oxide (NO), Inducible NO synthase (iNOS), Interferon- $\gamma$  (IFN- $\gamma$ )

## **INTRODUCTION**

The gastrointestinal epithelium is a dynamic tissue characterized by a high cellular turnover rate with a balance between cell proliferation and cell apoptosis, consequently leading to renewal of the entire intestinal epithelium every 3 to 5 days (9, 19). This single layer of cells lining the gut lumen acts as a barrier against harmful intraluminal entities, including foreign antigens, microorganisms and toxins, and also acts as a selective filter allowing the translocation of essential dietary nutrients, electrolytes and water. However, these physiological functions are occasionally impaired under pathological conditions such as inflammation and ischemia-reperfusion, and are accompanied by intestinal histological changes, including apoptosis.

Fasting is likely a physiological challenge evoking a response to the absence of luminal nutrients by functional and morphological changes, including intestinal epithelial apoptosis (8, 13, 21). However, prolonged fasting not only impairs intestinal physiological functions, but also brings about intestinal barrier dysfunction, including increased epithelial permeability and impaired tight junctions, subsequently leading to bacterial translocation in patients receiving a prolonged course of total parenteral nutrition (TPN) (56). Recent studies also show that proinflammatory cytokine-induced apoptosis causes loose epithelial tight junctions and an increase in paracellular permeability, raising a possibility of apoptosis-mediated intestinal barrier dysfunction (3, 44).

Among the many factors affecting the regulation of apoptosis, considerable attention has been given to the possible contribution of nitric oxide (NO) in the process of intestinal apoptosis (4, 35, 53, 57) and barrier dysfunction. Recent reports describing the link between NO and intestinal barrier functions demonstrated that inhibition of inducible NO synthase (iNOS) reduces bacterial translocation with a decrease in enterocyte apoptosis in LPS-induced rat intestinal injury (12), and improves intestinal barrier dysfunction induced by prolonged oral TPN feeding in rats (23).

According to recent knowledge, apoptosis is regulated through two distinct pathways converging to sequential activation of cysteine proteases of the caspase family, leading to the common final events of DNA-fragmentation (14, 33, 50). The intrinsic type-2 pathway occurs in response to diverse stresses, including ischemia-reperfusion via a mitochondria-mediated pathway following the release of cytochrome *c* from damaged mitochondria. On the other hand, fasting promotes intestinal mucosal apoptosis through ligand-mediated trimerization of death receptors of the tumor necrosis factor (TNF) family, that is, the so-called extrinsic pathway (type-1 apoptotic pathway). Although most reports have investigated the relationships of caspase activity and cytokine levels on intestinal apoptotic morphology in fasting animal models (2, 9, 16, 27), the NO contribution to fasting-mediated intestinal mucosal apoptosis remains to be elucidated, especially in the early phase of fasting. Therefore, the aim of the present study was to investigate the mechanism of fasting-induced intestinal apoptosis with respect to the role of NOS in the regulation of intestinal mucosal apoptosis during the early phase of fasting in rats.

## MATERIALS AND METHODS

### *Animals and experimental design*

The experimental protocol and design were approved by the Institutional Animal Care and Use Committee at the Life Science Center of Josai University and were consistent with the Guide for the Care and Use of Laboratory Animals published by the NIH. Male Wistar rats weighing 200-220 g (at 9 weeks of age) were purchased from SLC Inc. (Shizuoka, Japan), and were housed individually in wire-bottomed cages to prevent coprophagia, in a room illuminated from 7:00 a.m. to 7:00 p.m. (12:12-h light-dark cycle). The rats were allowed free access to deionized water and standard rat chow (CE-2, CLEA Japan) ad libitum until the study began. At 10 weeks of age, seventy rats were randomly divided into two groups (Fig. 1): saline (SA) group and aminoguanidine (AG) group. Each group was further divided into five subgroups as follows: 1) SA + ad libitum, 2) SA + 24-h fast, 3) SA + 48-h fast, 4) SA + 60-h fast, 5) SA + 72-h fast, 6) AG (a relatively selective iNOS inhibitor) + ad libitum, 7) AG + 24-h fast, 8) AG + 48-h fast, 9) AG + 60-h fast, 10) AG + 72-h fast. All groups were subcutaneously administered with SA or AG (20 mg/kg) (47), 18 h before, and 6, 30 and 54 h after fasting. The rats fasted for 24 h, 48 h, 60 h and 72 h underwent food withdrawal with only water being supplied. The rats were weighed every day.

We chose AG as an iNOS inhibitor. Although new iNOS inhibitors such as (1S, 5S, 6R,

7R)-2-aza-7-chloro-3-imino-5-methylbicyclo [4.1.0] heptane hydrochloride (ONO-1714) or N-(3-(aminomethyl)benzyl)acetamidine (1400W) have been developed and are being used as more selective iNOS inhibitors than AG in conditions such as sepsis-associated lung injury and lung dysfunction in endotoxemia (40, 58), accumulated references regarding the dose and timing of AG administration are available for consistent interpretation of inhibition studies of iNOS, especially in the intestine (46, 47, 48).

### ***Collection of intestinal mucosa***

After fasting with SA or AG, animals were anesthetized and then euthanized by exsanguination between 9.00 and 11.00 a.m. (except for 60-h fast: between 8.00 and 10.00 p.m.). The entire small intestine was carefully removed and placed on ice. The lumen of the intestine was flushed with 20 ml of ice-cold phosphate-buffered saline (PBS) to clear the intestinal lumen. The oral 10 cm part of the intestine was treated as the duodenum, and the rest of the intestine was divided into two segments representing proximal (jejunum) and distal (ileum) ends. The segments used for several analyses were the jejunum, from 3 to 5 cm distal to the duodenum (16). Some pieces, approximately 3 cm in length, were fixed in 10% neutral buffered formalin for measurement of mucosal height and for immunohistochemistry. Other segments were snap-frozen in liquid nitrogen and stored at -80 °C until use.

***Histopathological analysis, including apoptotic index, terminal deoxynucleotidyl transferase (TdT)-mediated dUDP-biotin nick-end labeling (TUNEL) staining and cell proliferation***

Tissue samples fixed in 10% neutral buffered formalin were then embedded in paraffin and sectioned. The specimens were stained with hematoxylin and eosin (HE). Mucosal height (villous height plus crypt depth) was measured using a microscope (Olympus BX41, Japan) and a digital camera system (Pixera Penguin 150CL, USA) for ad libitum-fed and fasted rats. Mucosal height was measured in at least 30 villi per animal.

In order to detect enterocyte apoptosis in the jejunal villus, both TUNEL staining and apoptotic index (AI) were used. TUNEL staining is easy to interpret over all images for apoptosis; however, because of its nonspecific staining (28), representative apoptotic changes were also detected for the analysis of AI using conventional light microscopy of HE-stained specimens. We followed the method described by Dahly, Guo, and Ney (11). In brief, jejunal sections were examined for apoptotic enterocytes in a blinded manner by an experimental pathologist (H.U.) based on the characteristic findings of apoptotic cells, including condensed chromatin, nuclear fragmentation, intensely eosinophilic cytoplasm and formation of apoptotic bodies (Fig. 6A). Fifty villus columns were assessed per rat (n=7 rats per subgroup). For each villus column assessed (i.e., one side of the villus in a longitudinal cross-section), the number and position of apoptotic cells, as well as the total number of cells in the villus column, were recorded. To account for the effects of fasting and AG treatment on apoptosis, the ratio of

apoptotic cells to one villus column and AI were determined. The mean number of apoptotic cells per villus column was calculated by dividing the total number of apoptotic cells in the well-oriented villus cell columns by 50 for each rat. In addition, AI was quantified by counting the total number of apoptotic cells in the 50 well-oriented villus columns and expressing this as the percentage of the total number of cells in the 50 villus columns for each rat.

To identify locations of apoptosis along the villus, AI distribution curves were constructed based on group means that plotted cell position vs. AI at each position. AI, in this case, was defined as the total number of apoptotic cells at each cell position expressed as the percentage of the total number of cells counted at that cell position.

Fragmented DNA was stained using the TUNEL method (17), with an Apoptosis in situ Detection KIT (Wako, Japan). The specimens were dewaxed and incubated with 20 µg/ml proteinase K for 20 min at 37 °C, the reaction was terminated with buffer containing bovine serum, and then the specimens were incubated for 5 min. PBS was applied directly on the specimens for 10 min at room temperature. Subsequently, 100 µl of terminal deoxynucleotidyl transferase (TdT) reaction solution was added, and the mixture was incubated at 37 °C for 25 min. In additional control sections, TdT reaction solution was omitted. The specimens were incubated successively with PBS containing 3% hydrogen peroxide for 20 min at room temperature to inactive endogenous peroxidases, and then were covered with 100 µl of horseradish peroxidase (POD)-conjugated antibody solution, and incubated for 10 min at 37 °C.

The specimens were soaked in PBS for 10 min, and then covered with 100  $\mu$ l of 3,3'-diaminobenzidine tetrahydrochloride (DAB) solution for 2 min at room temperature for color development. Finally, the specimens were counterstained with hematoxylin and examined with a light microscope. A minimum of 30 villi were randomly selected for TUNEL staining, and the number of TUNEL-positive cells was calculated. The TUNEL-positive rate was determined by dividing the number of cells by the total number of cells in the villi and multiplying by 200.

Crypt cell proliferation was assessed by using 5-bromo-2'-deoxyuridine (5-BrdU) incorporation to identify cells in the S phase of the cell cycle (49). 5-BrdU immunohistochemistry staining was performed by an anti-5-BrdU monoclonal antibody and a VECTASTAIN Elite ABC KIT (Vector Laboratories, USA). Rats were given intraperitoneal injections of 100 mg/kg 5-BrdU 60 min before sacrifice. The specimens were dewaxed and were immersed in 3% hydrogen peroxide-methanol solution for 20 min. The specimens were washed with PBS and denatured in 2N hydrochloric acid solution for 20 min. The specimens were washed with PBS and were immersed in 0.1M boric-acid buffer solution (pH 8.5) for pH control at 5 min. The specimens were incubated with 20  $\mu$ g/ml proteinase K for 25 min at 37 °C, the reaction was terminated with PBS containing bovine serum, and then the specimens were incubated for 5 min. The specimens were covered with 300  $\mu$ l of mouse anti-5-BrdU monoclonal antibody (1: 50; Chemicon International, CA) solution and incubated for 1 h at 37 °C. In additional control sections, the primary antibody was omitted. The specimens were covered with

biotinylated goat anti-mouse IgG antibody (1 : 200; Vector Laboratories, USA) solution. After the specimens were washed with PBS for 10 min, they were incubated with avidin-biotin-peroxidase complex solution for 1 h at room temperature. Color development was performed at room temperature in a substrate medium containing 0.05% DAB-H<sub>2</sub>O<sub>2</sub> solution. Finally, the specimens were counterstained with hematoxylin. The number of labeled cells in at least 10 well-oriented longitudinal crypts in each sample was determined under a light microscope. The result is shown as the number of 5-BrdU-labeled cells among the crypt cells.

### ***Immunohistochemistry of iNOS***

Immunohistochemical staining of iNOS was performed with an anti-iNOS polyclonal antibody and a VECTASTAIN Elite ABC KIT (Vector Laboratories, USA) (32). The specimens obtained from the jejunum after 24-h, 48-h, and 72-h fasting as well as ad libitum rats were dewaxed and treated for antigen retrieval by boiling in 10 mM citrate buffer (pH 6.0) for 20 min at 95 °C (44). After being washed with PBS, sections were incubated in 6% hydrogen peroxide for 1 h and washed again with PBS. Nonspecific binding was blocked with a 20% goat serum solution in PBS for 10 min at room temperature. Sections were incubated with rabbit anti-iNOS polyclonal antibody (1:100; BD Transduction Laboratories, USA). In additional control sections, the primary antibody was omitted. A biotinylated goat anti-rabbit IgG (1:200; VECTASTAIN, USA) was used as a secondary antibody. Sections were then treated with VECTASTAIN Elite

ABC KIT, and reaction products were detected using color development at room temperature in a substrate medium containing a 0.05% DAB-H<sub>2</sub>O<sub>2</sub> solution. Finally, the specimens were counterstained with hematoxylin and examined with a light microscope and a digital camera system.

### ***Nitrite concentrations in jejunum***

Tissue samples stored at -80 °C were measured for nitrite concentrations using a dedicated HPLC system (ENO-20; EiCom, Japan). This method is based on the separation of nitrite and nitrate by ion chromatography, followed by on-line reaction of nitrate to nitrite, post-column derivatization with Griess reagent, and detection at 540 nm. Proteins in each sample were removed by centrifugation at 10,000 g for 5 min following methanol precipitation (jejunum : methanol = 1 : 2 weight/volume, 4 °C) (26).

### ***Analysis of iNOS, neuronal NOS (nNOS) and interferon-gamma (IFN- $\gamma$ ) mRNA expression by reverse transcription-polymerase chain reaction (RT-PCR)***

Tissue samples stored at -80 °C were extracted using TaKaRa RNAiso Reagent (TaKaRa Bio, Japan) according to the manufacturer's instructions. Total RNA concentrations were quantified by spectrophotometry at 260 nm. RT-PCR was performed with 1 mg of total RNA using an RNA PCR kit (AMV) Ver. 3.0 (TaKaRa Bio, Japan) according to the manufacturer's instructions: 1

cycle at 42 °C for 30 min, 99 °C for 5 min, and 5 °C for 5 min for reverse transcription; and 30 cycles at 94 °C for 30 sec, 60 °C for 30 sec, and 72 °C for 1 min for PCR. PCR was performed using a RoboCycler 96 gradient temperature cyler (Stratagene, CA). The oligonucleotides used as primers were synthesized by TaKaRa Bio, Japan. The primer pairs were designed as follows (product size and Primer ID provided by TaKaRa Bio are shown in parentheses): iNOS forward primer, 5'-ctcactgtggctgtggcaccta-3'; and iNOS reverse primer, 5'-gggtcttcgggcttcaggta-3' (101 bp, RA008296). In addition, because intraepithelial lymphocyte (IEL)-derived IFN- $\gamma$  is reported to evoke enterocyte apoptosis with parenteral nutrition (55), we considered a possible involvement of IFN- $\gamma$  in fasting-induced apoptosis. We therefore performed RT-PCR for IFN- $\gamma$ : IFN- $\gamma$  forward primer, 5'-aggccatcagcaacaacataagtg-3'; reverse primer, 5'-gacagctttgtgctggatctgtg-3' (140 bp, RA021293). Based on recent reports showing nNOS involvement in the regulation of iNOS expression in the small intestine (18, 39), we also performed additional RT-PCR for nNOS: nNOS forward primer, 5'-tcaaagccatccagcgcata-3'; and nNOS reverse primer, 5'-gcggttggtcacttcatacgttc-3' (146 bp, RA022317). Target mRNA expressions were quantified relative to the expression of glyceraldehyde-3-phosphate dehydrogenase (GAPDH): GAPDH forward primer, 5'-ggcacagtcaaggctgagaatg-3'; and GAPDH reverse primer, 5'-atggtggtgaagacgccagta-3' (143 bp, RA015380). A portion of each PCR mixture was electrophoresed in 2% agarose gel in TBE buffer (89 mM Tris, 89 mM boric acid, 2 mM EDTA, pH 8.3), and the gel was visualized by ethidium bromide staining. The intensity of

the PCR products was measured using a Gene Genius Bioimaging System (SYNGENE, UK), and the ratios of iNOS, nNOS and IFN- $\gamma$  expression relative to GAPDH expression were calculated for each sample.

### *DNA oxidation analysis*

The generation of reactive oxygen species (ROS) in the jejunum was estimated by 8-hydroxydeoxyguanosine (8-OHdG) levels in DNA (24). 8-OHdG is a product of oxidative DNA damage following specific enzymatic cleavage after 8-hydroxylation of the guanine base and has been proposed as an index of oxidative DNA damage reflecting the repair rate from DNA (45). Jejunal DNA was purified by DNA Extractor TIS Kit (Wako, Japan) using sodium iodide (NaI) as a chaotropic agent and an oxidation inhibitor. DNA was pretreated as follows: 200  $\mu$ g of sample, obtained by DNA preparation from the jejunum of a rat, was dissolved in 135  $\mu$ l of water, and after addition of 15  $\mu$ l 200 mM sodium acetate containing 6 units of nuclease P1 (Wako, Japan), samples were incubated for 1 h at 37 °C. Fifteen microliters of 1 M Tris-HCl buffer, pH 7.4, and 2 units of alkaline phosphatase (Wako, Japan) were then added and incubation was continued for 1 h. Hydrolysates were filtered through a VIVASPIN 500 MWCO 10,000 (Sartorius Stedim, Germany) device at 14,000 rpm for 10 min, and 50  $\mu$ l of filtrate was applied to the wells of the ELISA plate. The levels of 8-OHdG in the samples were determined with an ELISA kit (Japan Institute for the Control of Aging, Shizuoka, Japan). The kit can

measure extremely low levels of 8-OHdG, and the specificity of the monoclonal antibody has been established (41). The wells were subjected to optical density measurement at 450 nm. 8-OHdG ELISA was performed in triplicate and the means were calculated. The data, expressed as picograms of 8-OHdG per microgram of DNA, were calculated on the basis of a linear calibration curve generated for each experiment with 8-OHdG standard solutions.

### ***Statistical analysis***

Statistical analyses were performed using Dr SPSS II for Windows. All values are expressed as means  $\pm$  SE. One-way ANOVA followed by a Bonferroni multiple comparisons test was used for analyzing the statistical difference between the fasting periods in SA- or AG-treated groups. Two-way ANOVA followed by a Bonferroni multiple comparisons test was used for analyzing the statistical difference between the SA- and AG-treated groups for the fasted periods. Statistical significance was accepted at a value of  $P < 0.05$ .

## **RESULTS**

### ***Body weight changes***

Figure 2 shows body weight changes expressed as the ratio of after/before fasting in SA-treated and AG-treated rats. Gradual decreases in body weight both in SA- and AG-treated

groups were observed along with fasting. Rats fasted for 72 h with SA and AG treatment showed an approximately 19% ( $P < 0.05$ ) and 18% ( $P < 0.05$ ) body weight loss, respectively, compared to ad libitum-fed control rats. There was no significant difference in weight loss at each fasting period between the SA and AG treatment, suggesting AG has no impact on fasting-induced body weight loss.

### ***Histological characterization of jejunal mucosal atrophy in fasted rats treated with SA or AG***

Decreasing jejunal mucosal height both in SA- and AG-treated rats was observed along with fasting. However, significant differences ( $P < 0.05$ ) in jejunal mucosal height were found between the SA- and AG-treated rats at 48 h, 60 h, and 72 h fasting periods, suggesting that AG significantly inhibited progressive jejunal mucosal atrophy in fasted rats (Fig. 3).

In order to evaluate how reduced cell proliferation and/or increased cell apoptosis contributes to jejunal mucosal atrophy, we assessed 5-BrdU incorporation to the cells and TUNEL staining of the jejunum, indicative of cell proliferation and apoptosis in the jejunum, respectively. Although decreases in cell proliferation along with fasting were observed irrespective of the presence or absence of AG (Fig. 4), fasting remarkably induced jejunal cell apoptosis, which was completely inhibited by AG over all of the fasting periods as observed by TUNEL staining and TUNEL-positive rate (Figs. 5A and 5B). Conventional light microscopy for detecting representative apoptotic changes also showed an increased ratio of apoptotic cells to one villus

column and AI (6.8- to 8.6-fold increase:  $P < 0.05$ ) in fasted rats with SA, as well as significant inhibitory effects of AG on fasting-induced apoptosis over the indicated fasting periods (Table 1). For better identification of locations of apoptosis along the villus compartments, AI distribution curves were constructed by detecting representative apoptotic changes by conventional light microscopy of HE-stained specimens. Although many TUNEL-positive cells were observed in the tip of the jejunal villus in fasted rats (Fig. 5A), AI distribution curves showed increased apoptosis throughout the whole jejunal villus of fasted rats, with peak incidence of apoptosis in the bottom half of the villus compared to ad libitum-fed rats (Fig. 6B). Similar to the inhibitory effect of AG on AI, decreases in apoptosis by AG treatment were also observed in the AI distribution curves (Fig. 6B).

### ***Nitrite levels in the jejunum***

Similar to the inhibitory effect of AG on intestinal apoptosis, AG, a selective iNOS inhibitor, also significantly inhibited the increasing accumulation of intestinal nitrite, a stable oxidation product of endogenous NO, especially in fasting (Fig. 7), suggesting that iNOS-induced NO might act as an important mediator of intestinal apoptosis in fasting rats.

### ***Intestinal transcriptional expression of iNOS and IFN- $\gamma$***

Next, we tried to demonstrate the causative effect of iNOS on intestinal apoptosis by

evaluating transcriptional levels of iNOS during fasting. Figure 8 shows that fasting induced iNOS mRNA, which was suppressed by AG. Because of intimate anatomical localization of IEL located at basolateral surfaces of intestinal epithelial cells (IEC), possibly implicating a functional dialogue between the two cells, recent reports indicated phenotypic changes of IEC during administration of total parenteral nutrition via IEL-derived cytokines such as IFN- $\gamma$  (54, 55, 59). We therefore investigated the effects of fasting and AG treatment on transcriptional expression of IFN- $\gamma$ . Figure 9 shows that fasting induced IFN- $\gamma$  mRNA, which was also inhibited by AG, possibly suggesting that iNOS-related transcriptional induction of IFN- $\gamma$  following fasting might exist in the intestinal mucosa.

### ***Immunohistochemical localization of iNOS***

Immunostaining for iNOS was performed to localize the expression of iNOS protein in the jejunum. The ad libitum rats revealed negligible iNOS staining in the crypts and little positive staining was recognized in the cytoplasm at the villus-tip epithelial cells (Fig. 10 A-1 and A-2). These findings diminished with AG treatment in ad libitum fed rats (Fig. 10 B-1 and B-2). However, 24-h fasting showed heavily positive iNOS immunostaining along the mucosal epithelial monolayer of the jejunum (Fig. 10 C-1 and C-2). These iNOS immunoreactivities were almost completely inhibited by AG treatment (Fig. 10 D-1 and D-2). Similar results were observed in 48-h and 72-h fasting. In addition, the distribution of iNOS protein expressed along

with villus is histologically consistent with that of cell apoptosis observed in the histomorphometric assessment (Fig. 6B).

### ***Intestinal transcriptional expression of nNOS***

As there are reports showing that nNOS plays an important role in the regulation of iNOS expression in the small intestine of fasting animal models (18, 39), intestinal transcriptional levels of nNOS were also investigated to evaluate the effect of fasting on nNOS transcription in the jejunum. In contrast to the fasting-induced increase in iNOS mRNA and protein expression (Figs. 8 and 10), a reduced nNOS transcription after fasting was observed (Fig. 11), possibly suggesting a reverse relationship between nNOS and iNOS at least at the transcriptional level.

### ***Intestinal DNA oxidative damage***

The 8-OHdG levels were also investigated to evaluate the effect of fasting on the ROS generation in the jejunum (Fig. 12). In SA-treated groups, fasting increased jejunal 8-OHdG levels at 24 h, 48 h, and 72 h fasting periods compared with the ad libitum-fed rats ( $P < 0.05$ ). AG significantly ( $P < 0.05$ ) inhibited the fasting-induced increases in the jejunal 8-OHdG levels at 48 and 72 h fasting periods compared with the respective SA-treated group at each fasting period. Considering the AG inhibitory effect on increased IFN- $\gamma$  induction and ROS production after fasting (Fig. 9, 12), iNOS-induced NO might play a central role upstream in the process of

fasting-induced apoptosis in which IFN- $\gamma$  and ROS might be involved.

## **DISCUSSION**

Gut mucosal homeostasis depends on a balance between cell proliferation and cell death (15, 27, 37). In the present study, incremental fasting resulted in jejunal mucosal atrophy caused by both decreased crypt stem cell proliferation and increased villus cell apoptosis. We applied TUNEL staining for detection of apoptotic cells (9). TUNEL staining allows easy observation of apoptotic distribution over tissue sections; however, because of its nonspecific staining (28), we also used conventional light microscopy for detection of characteristic apoptotic changes in HE-stained specimens. This method is extremely precise and presently considered the reference standard (36) if representative morphologic changes are observed (22). Consistent with the results from TUNEL-positive rate, we observed fasting-induced apoptosis and its improvement with AG using this histomorphometric assessment. However, the distribution of apoptotic cells is spread throughout the whole villus with predominant localization at the bottom one-half of the villus in the histomorphometric assessment (Fig. 6B), whereas apoptosis is confined to the top one-half of the villus in TUNEL staining (Fig. 5A), despite using carefully controlled techniques on rapidly fixed tissues to avoid nonspecific staining. It has been suggested by Merritt et al that senescent cell suicide particularly evident on the villus tip may have different temporal and even

genetic regulation from that of damage-induced apoptosis observed in the crypts treated with irradiation or TPN (11, 31). The difference in methodology between histomorphometric assessment and TUNEL staining might have some influence on the localizations of apoptotic cells in the villi, as observed in the present study. The precise mechanism involved still remains to be elucidated, and further investigation will be required to interpret this issue.

In the present study, we indicated that fasting-induced apoptosis might be mediated by iNOS, which is supported by increasing tissue levels of nitrite (Fig. 7), the stable oxidation product of endogenous NO especially in fasting, and the increase in both transcriptional and protein levels of iNOS in atrophied jejunal mucosa observed as early as 24 h after fasting (Figs. 8 and 10). In order to examine how iNOS-induced NO may be related to fasting-induced apoptosis, an iNOS inhibition study was also carried out using AG, a selective iNOS inhibitor. Decreasing jejunal mucosal height with progressive fasting was significantly inhibited by AG (Fig. 3), which suppressed mucosal cell apoptosis without having any effects on the decreasing cell proliferation index (Fig. 4). We are convinced that iNOS plays a central role in fasting-induced intestinal apoptosis, because AG treatment histologically improved apoptosis (Figs. 5 and 6) accompanied with inhibition of increased iNOS transcription and protein expression (Figs. 8 and 10), increased ROS production (Fig. 12) and increased IFN- $\gamma$  transcription (Fig. 9) following fasting, suggesting that iNOS-induced NO might be working upstream in the process of fasting-induced apoptosis (Fig. 13).

The causative effect of NO on apoptosis has been well documented. Depending on cell types and NO concentrations at the site where NO is produced, NO is a bifunctional regulator of apoptosis (7, 29). Low levels of NO exposure through the activation of endogenous NOS and slow release rates from NO donors are associated with anti-apoptotic effects, whereas under some conditions such as inflammation or neurodegenerative diseases, NO-dependent apoptosis (pro-apoptotic) has been observed (6). Recently, it has been clearly demonstrated that ischemia/reperfusion-induced apoptosis as a pathological state is related to the type-2 apoptosis pathway, in which cytochrome c release from the mitochondria triggers intrinsic apoptosis by opening mitochondrial permeability transition pores (16, 52).

Although the role of NO in the regulation of fasting-induced apoptosis has been less well documented so far, we considered that this apoptosis might be mediated by the type-1 death-pathway, mainly based on the previous observation by Fujise et al (16) using the same experimental setting as in our present study. From our present results, we cannot determine whether NO works via type-1 death-pathway-mediated apoptosis. However, if we pay attention to IFN- $\gamma$ , we are able to hypothesize that ROS-mediated IFN- $\gamma$  might induce intestinal apoptosis through the type-1 death-pathway, because ROS is a main inducer of IFN- $\gamma$  from IEL in the intestine. We therefore performed additional experiments examining a possible contribution of ROS in iNOS-induced apoptosis by measuring 8-OHdG levels, consequently showing an increased intestinal ROS production following fasting, which was reversed by AG treatment (Fig.

12), indicating a ROS-involved mechanism in this iNOS-induced apoptosis pathway (Fig. 13). Recent evidence shows that IEL-derived IFN- $\gamma$  evokes enterocyte apoptosis via an up-regulation of Fas/FasL, leading to the increase in sensitivity of epithelial cells to Fas-mediated apoptosis (30, 55) through the type-1 pathway (55). It has been suggested that complex reciprocal interactions exist between IEC and IEL (20, 55); therefore, it is likely that IEC and IEL form a reciprocal feedback loop in which iNOS-released NO, physiologically present in IEC, stimulates IFN- $\gamma$  production in IEL through a ROS-mediated mechanism (1, 5, 38), then IFN- $\gamma$  stimulates further iNOS-derived NO production, resulting in further IFN- $\gamma$  production and subsequent IEC apoptosis (Fig. 13).

Since AG, a selective iNOS inhibitor, generally inhibits iNOS activity via binding to its active centre according to its crystal structural analysis (10), the inhibition may act at the post-translational rather than at the transcriptional level. Our present study, however, showed that AG inhibited fasting-induced iNOS both in mRNA and protein levels, accompanied with the decrease in transcription of IFN- $\gamma$ . As mentioned above, taking into consideration the close proximity and interaction between IEL and IEC, there could be a situation where NO induction by IEC and IFN- $\gamma$  by IEL affect each other via a reciprocal mechanism (Fig. 13). Therefore, iNOS inhibition by AG suppresses NO-mediated IFN- $\gamma$  transcription, followed by the decrease in iNOS transcription as well.

Another important issue to be discussed is how fasting induces intestinal iNOS expression.

Although little has been confirmed so far regarding the cause-and-effect relationship between fasting and iNOS, Qu and colleagues recently showed nNOS involvement in the regulation of iNOS expression in the rat small intestine. They demonstrated that nNOS, the predominant form (>90%) expressed in the rat small intestine, physiologically suppresses the gene expression of constitutive iNOS in IEC through nuclear factor kappa B (NF- $\kappa$ B) down-regulation, and also that nNOS suppression leads to I $\kappa$ B $\alpha$  degradation, followed by NF- $\kappa$ B activation and a subsequent increase in iNOS expression (39). Grongnet further showed that the intestinal nNOS expression is drastically reduced by fasting in the piglet jejunum (18). Consistent with these reports, we observed a reduced nNOS transcription after fasting (Fig. 11) with an increase in iNOS transcription (Fig. 8), suggesting a possible nNOS-involved mechanism underlying fasting-induced iNOS expression in our model (Fig. 13). However, although several other physiological factors, including leptin (51) and the feeding center such as the ventromedial hypothalamus (42), absence of luminal nutrients (16, 25) and mechanical stimuli (27), and reduced intestinal blood flow (16, 34) have also been reported to be involved in the regulation of apoptosis in the rat small intestine, further studies are needed to clarify the causative mechanism of iNOS expression in a fasting rat model.

In conclusion, these results suggest that fasting induces intestinal apoptosis through an iNOS-mediated mechanism, and that a close interaction could exist between iNOS and IFN- $\gamma$  in the intestinal mucosa, affecting each other, and leading to intestinal apoptosis in fasting rats.

## GRANTS

This work was supported by The Ministry of Education, Culture, Sports, Science and Technology of Japan under Exploratory Research Grant-In-Aid 19659347 (to H. Uchida).

## REFERENCES

- 1. Abdeen S, Mathew TC, Khan I, Dashti H, and Asfar S.** Fasting-induced intestinal damage is mediated by oxidative and inflammatory responses. *Br J Surg* 96: 552-559, 2009.
- 2. Adams SD, Delano BA, Helmer KS, and Mercer DW.** Fasting exacerbates and feeding diminishes LPS-induced liver injury in the rat. *Dig Dis Sci* 54: 767-773, 2009.
- 3. Bojarski C, Bendfeldt K, Gitter AH, Mankertz J, Fromm M, Wagner S, Riecken EO, and Schulzke JD.** Apoptosis and intestinal barrier function. *Ann NY Acad Sci* 915: 270-274, 2000.
- 4. Boscá L and Hortelano S.** Mechanisms of nitric oxide-dependent apoptosis: involvement of mitochondrial mediators. *Cell Signal* 11: 239-244, 1999.
- 5. Boza JJ, Moënnos D, Vuichoud J, Jarret AR, Gaudard-de-Weck D, Fritsché R, Donnet A, Schiffrin EJ, Perruisseau G, and Ballèvre O.** Food deprivation and refeeding influence growth, nutrient retention and functional recovery of rats. *J Nutr* 129: 1340-1346, 1999.
- 6. Brookes PS, Salinas EP, Darley-USmar K, Eiserich JP, Freeman BA, Darley-USmar VM, and Anderson PG.** Concentration-dependent effects of nitric oxide on mitochondrial

permeability transition and cytochrome *c* release. *J Biol Chem* 275: 20474-20479, 2000.

7. **Brüne B, Knethen AV, and Sandau KB.** Nitric oxide (NO): an effector of apoptosis. *Cell Death Differ* 6: 969-975, 1999.
8. **Carey HV, Hayden UL, and Tucker KE.** Fasting alters basal and stimulated ion transport in piglet jejunum. *Am J Physiol Regul Integr Comp Physiol* 267; R156-R163, 1994.
9. **Chappell VL, Thompson MD, Jeschke MG, Chung DH, Thompson JC, and Wolf SE.** Effects of incremental starvation on gut mucosa. *Dig Dis Sci* 48: 765-769, 2003.
10. **Crane BR, Arvai AS, Gachhui R, Wu C, Ghosh DK, Getzoff ED, Stuehr DJ, and Tainer JA.** The structure of nitric oxide synthase oxygenase domain and inhibitor complexes. *Science* 278: 425-431, 1997.
11. **Dahly EM, Guo Z, and Ney DM.** Alterations in enterocyte proliferation and apoptosis accompany TPN-induced mucosal hypoplasia and IGF-I-induced hyperplasia in rats. *J Nutr* 132: 2010-2014, 2002.
12. **Dickinson E, Tuncer R, Nadler E, Boyle P, Alber S, Watkins S, and Ford H.** NOX, a novel nitric oxide scavenger, reduces bacterial translocation in rats after endotoxin challenge. *Am J Physiol Gastrointest Liver Physiol* 277: G1281-G1287, 1999.
13. **Dunel-Erb S, Chevalier C, Laurent P, Bach A, Decrock F, and Maho Y Le.** Restoration of the jejunal mucosa in rats refed after prolonged fasting. *Comp Biochem Physiol A Mol Integr Physiol* 129: 933-947, 2001.

- 14. Feinstein E, Kimchi A, Wallach D, Boldin M, and Varfolomeev E.** The death domain: a module shared by proteins with diverse cellular functions. *Trends Biochem Sci* 20: 342-344, 1995.
- 15. Fujimoto K, Iwakiri R, Wu B, Fujise T, Tsunada S, and Ootani A.** Homeostasis in the small intestinal mucosa balanced between cell proliferation and apoptosis is regulated partly by the central nervous system. *J Gastroenterol* 37 [Suppl 14]:139-144, 2002.
- 16. Fujise T, Iwakiri R, Wu B, Amemori S, Kakimoto T, Yokoyama F, Sakata Y, Tsunada S, and Fujimoto K.** Apoptotic pathway in the rat small intestinal mucosa is different between fasting and ischemia-reperfusion. *Am J Physiol Gastrointest Liver Physiol* 291: G110-G116, 2006.
- 17. Gavrieli Y, Sherman Y, and Ben-Sasson SA.** Identification of programmed cell death in situ via specific labeling of nuclear DNA fragmentation. *J Cell Biol* 119: 493-501, 1992.
- 18. Grongnet JF, and David JC.** Reciprocal variations of nNOS and HSP90 are associated with fasting in gastrointestinal tract of the piglet. *Dig Dis Sci* 48: 365-372, 2003.
- 19. Hall PA, Coates PJ, Ansari B, and Hopwood D.** Regulation of cell number in the mammalian gastrointestinal tract: the importance of apoptosis. *J Cell Sci* 107: 3569-3577, 1994.
- 20. Hoffman RA.** Intraepithelial lymphocytes coinduce nitric oxide synthase in intestinal epithelial cells. *Am J Physiol Gastrointest Liver Physiol* 278: G886-G894, 2000.

- 21. Holt PR, Wu S, and Yeh KY.** Ileal hyperplastic response to starvation in the rat. *Am J Physiol Gastrointest Liver Physiol* 251: G124-G131, 1986.
- 22. Hotchkiss RS, Schmiege RE Jr, Swanson PE, Freeman BD, Tinsley KW, Cobb JP, Karl IE, and Buchman TG.** Rapid onset of intestinal epithelial and lymphocyte apoptotic cell death in patients with trauma and shock. *Crit Care Med* 28: 3207-3217, 2000.
- 23. Hsu CM, Liu CH, and Chen LW.** Nitric oxide synthase inhibitor ameliorates oral total parenteral nutrition-induced barrier dysfunction. *Shock* 13: 135-139, 2000.
- 24. Inoue S, and Kawanishi S.** Oxidative DNA damage induced by simultaneous generation of nitric oxide and superoxide. *FEBS Lett* 371: 86-88, 1995.
- 25. Iwakiri R, Gotoh Y, Noda T, Sugihara H, Fujimoto K, Fuseler J, and Aw TY.** Programmed cell death in rat intestine: effect of feeding and fasting. *Scand J Gastroenterol* 36: 39-47, 2001.
- 26. Janero DR, Bryan NS, Saijo F, Dhawan V, Schwalb DJ, Warren MC, and Feelisch M.** Differential nitros(yl)ation of blood and tissue constituents during glyceryl trinitrate biotransformation in vivo. *Proc Natl Acad Sci USA* 101: 16958-16963, 2004.
- 27. Kakimoto T, Fujise T, Shiraishi R, Kuroki T, Park JM, Ootani A, Sakata Y, Tsunada S, Iwakiri R, and Fujimoto K.** Indigestible material attenuated changes in apoptosis in the fasted rat jejunal mucosa. *Exp Biol Med* 233: 310-316, 2008.
- 28. Kerr JF, Gobe GC, Winterford CM, and Harmon BV.** Anatomical methods in cell death.

*Methods Cell Biol* 46: 1-27, 1995.

- 29. Kim YM, Bombeck CA, and Billiar TR.** Nitric oxide as a bifunctional regulator of apoptosis. *Circ Res* 84: 253-256, 1999.
- 30. Martin CA and Panja A.** Cytokine regulation of human intestinal primary epithelial cell susceptibility to Fas-mediated apoptosis. *Am J Physiol Gastrointest Liver Physiol* 282: G92-G104, 2002.
- 31. Merritt AJ, Potten CS, Kemp CJ, Hickman JA, Balmain A, Lane DP, and Hall PA.** The role of *p53* in spontaneous and radiation-induced apoptosis in the gastrointestinal tract of normal and *p53*-deficient mice. *Cancer Res* 54: 614-617, 1994.
- 32. Morin MJ, Karr SM, Faris RA, and Gruppuso PA.** Developmental variability in expression and regulation of inducible nitric oxide synthase in rat intestine. *Am J Physiol Gastrointest Liver Physiol* 281: G552-G559, 2001.
- 33. Nagata S.** Apoptosis by death factor. *Cell* 88: 355-365, 1997.
- 34. Niinikoski H, Stoll B, Guan X, Kansagra K, Lambert BD, Stephens J, Hartmann B, Holst JJ, and Burrin DG.** Onset of small intestinal atrophy is associated with reduced intestinal blood flow in TPN-fed neonatal piglets. *J Nutr* 134: 1467-1474, 2004.
- 35. Piacenza L, Peluffo G, and Radi R.** L-Arginine-dependent suppression of apoptosis in *Trypanosoma cruzi*: Contribution of the nitric oxide and polyamine pathways. *Proc Natl Acad Sci USA* 98: 7301-7306, 2001.

- 36. Potten CS.** What is an apoptotic index measuring? A commentary. *Br J Cancer* 74: 1743-1748, 1996.
- 37. Potten CS and Booth C.** The role of radiation-induced and spontaneous apoptosis in the homeostasis of the gastrointestinal epithelium: a brief review. *Comp Biochem Physiol B Biochem Mol Biol* 118: 473-478, 1997.
- 38. Pyo CW, Lee SH, and Choi SY.** Oxidative stress induces PKR-dependent apoptosis via IFN- $\gamma$  activation signaling in Jurkat T cells. *Biochem Biophys Res Com* 377: 1001-1006, 2008.
- 39. Qu XW, Wang H, De Plaen IG, Rozenfeld RA, and Hsueh W.** Neuronal nitric oxide synthase (NOS) regulates the expression of inducible NOS in rat small intestine via modulation of nuclear factor kappa B. *FASEB J* 15: 439-446, 2001.
- 40. Rudkowski JC, Barreiro E, Harfouche R, Goldberg P, Kishta O, D'Orleans-Juste P, Labonte J, Lesur O, and Hussain SNA.** Roles of iNOS and nNOS in sepsis-induced pulmonary apoptosis. *Am J Physiol Lung Cell Mol Physiol* 286: L793-L800, 2004.
- 41. Saito S, Yamaguchi H, Hasui Y, Kurashige J, Ochi H, and Yoshida K.** Quantitative determination of urinary 8-hydroxydeoxyguanosine (8-OHdG) by using ELISA. *Res Commun Mol Pathol Pharmacol* 107: 39-44, 2000.
- 42. Sakata H, Ootani A, Fujise T, Sakata Y, Wu B, Tsunada S, Iwakiri R, Fujimoto K, and Shiraishi T.** Decreased apoptosis and increased ornithine decarboxylase activity in the intestinal mucosa of rats with bilateral ventromedial hypothalamus lesions. *J Gastroenterol*

40: 137-142, 2005.

- 43. Schulzke JD, Bojarski C, Zeissig S, Heller F, Gitter AH, and Fromm M.** Disrupted barrier function through epithelial cell apoptosis. *Ann NY Acad Sci* 1072: 288-299, 2006.
- 44. Shi SR, Chaiwun B, Young L, Cote RJ, and Taylor CR.** Antigen retrieval technique utilizing citrate buffer or urea solution for immunohistochemical demonstration of androgen receptor in formalin- fixed paraffin sections. *J Histochem Cytochem* 41: 1599-1604, 1993.
- 45. Shigenaga M.K, Gimeno C.J, and Ames B.N.** Urinary 8-hydroxy-20-deoxyguanosine as a biological marker of in vivo oxidative DNA damage. *Proc. Natl. Acad. Sci. USA* 86: 9697–9701, 1989.
- 46. Sorrells DL, Friend C, Koltuksuz U, Courcoulas A, Boyle P, Garrett M, Watkins S, Rowe MI, and Ford HR.** Inhibition of nitric oxide with aminoguanidine reduces bacterial translocation after endotoxin challenge in vivo. *Arch Surg* 131: 1155-1163, 1996.
- 47. Takeuchi K, Hatazawa R, Tanigami M, Tanaka A, Ohno R, and Yokota A.** Role of endogenous nitric oxide (NO) and NO synthases in healing of indomethacin-induced intestinal ulcers in rats. *Life Sciences* 80: 329-336, 2007.
- 48. Tanaka A, Kunikata T, Mizoguchi H, Kato S, and Takeuchi K.** Dual action of nitric oxide in pathogenesis of indomethacin-induced small intestinal ulceration in rats. *J Physiol Pharmacol* 50: 405-17, 1999.
- 49. Tang Y, Swartz-Basile DA, Swietlicki EA, Yi L, Rubin DC, and Levin MS.** Bax is

required for resection-induced changes in apoptosis, proliferation, and members of the extrinsic cell death pathways. *Gastroenterology* 126: 220-230, 2004.

**50. Tsujimoto Y and Shimizu S.** Bcl-2 family: Life-or-death switch. *FEBS Lett* 466: 6-10, 2000.

**51. Utsumi H, Iwakiri R, Wu B, Fujise T, Sakata H, Shimoda R, Amemori S, Tsunada S, Ootani A, and Fujimoto K.** Intracerebroventricular administration of leptin-induced apoptosis in the rat small intestinal mucosa. *Exp Biol Med* 228: 1239-1244, 2003.

**52. Wu B, Iwakiri R, Tsunada S, Utsumi H, Kojima M, Fujise T, Ootani A, and Fujimoto K.** iNOS enhances rat intestinal apoptosis after ischemia-reperfusion. *Free Radical Bio Med* 33: 649-658, 2002.

**53. Xie K and Huang S.** Contribution of nitric oxide-mediated apoptosis to cancer metastasis inefficiency. *Free Radic Biol Med* 34: 969-986, 2003.

**54. Yang H, Finaly R and Teitelbaum DH.** Alteration in epithelial permeability and ion transport in a mouse model of total parenteral nutrition. *Crit Care Med* 31: 118, 2003.

**55. Yang H, Fan Y, and Teitelbaum DH.** Intraepithelial lymphocyte-derived interferon- $\gamma$  evokes enterocyte apoptosis with parenteral nutrition in mice. *Am J Physiol Gastrointest Liver Physiol* 284: G629-G637, 2003.

**56. Yang H, Feng Y, Sun X, and Teitebaum DH.** Enteral versus parenteral nutrition: Effect on intestinal barrier function. *Ann NY Acad Sci* 1165: 338-346, 2009.

- 57. Yuan B, Ohyama K, Bessho T, and Toyoda H.** Contribution of inducible nitric oxide synthase and cyclooxygenase-2 to apoptosis induction in smooth chorion trophoblast cells of human fetal membrane tissues. *Biochem Biophys Res Commun* 341: 822-827, 2006.
- 58. Yuba T, Nagata K, Yamada T, Osugi S, Kuwahara H, Iwasaki Y, Handa O, Naito Y, Fushiki S, Yoshikawa T, and Marunaka Y.** A novel potent inhibitor of inducible nitric oxide synthase, ONO-1714, reduces hyperoxic lung injury in mice. *Respir Med* 101: 793-799, 2007.
- 59. Wildhaber BE, Yang H, Spencer AU, Drongowski RA, and Teitelbaum DH.** Lack of enteral nutrition—effects on the intestinal immune system. *J Surg Res* 123: 8-16, 2005.

## LEGENDS

### *Figure 1. Experimental Design.*

Seventy male Wistar rats were divided into two groups. Thirty-five rats in each group received SA or AG (20 mg/kg) subcutaneously 18 h before fasting, and were randomly subdivided into 5 subgroups, including a normally-fed control group, according to fasting durations in each group: 1) SA + ad libitum (normally-fed control), 2) SA + 24-h fast, 3) SA + 48-h fast, 4) SA + 60-h fast, 5) SA + 72-h fast, 6) AG + ad libitum (normally-fed control), 7) AG + 24-h fast, 8) AG + 48-h fast, 9) AG + 60-h fast, 10) AG + 72-h fast. All rats received SA or AG subcutaneously, 6, 30 and 54 h after fasting. The large block arrows represent treatment with SA (open block arrow) and AG (closed block arrow). At the appointed time after fasting, intestinal tissues were collected. Seven rats were tested in each group.

### *Figure 2. Body weight changes expressed as the ratio of after/before fasting in SA-treated rats and AG-treated rats.*

Fasting caused gradual decreases in body weight both in SA- and AG- treated groups. There was no difference in weight loss between the SA and AG treatment at each fasting period. Values are means  $\pm$  SE. <sup>a</sup>P < 0.05 compared with the ad libitum-fed rats in SA-treated group. Seven rats were tested in each group. Open bars: SA-treated rats; closed bars: AG-treated rats.

*Figure 3. Effect of fasting and AG treatment on jejunal mucosal height.*

Although fasting caused gradual decreases in jejunal mucosal height both in SA- and AG-treated rats, there were significant differences ( $P < 0.05$ ) in jejunal mucosal height between the SA- and AG-treated rats at 48 h, 60 h, and 72 h fasting periods. Values are means  $\pm$  SE. <sup>a</sup> $P < 0.05$  compared with the ad libitum-fed rats in SA-treated group. <sup>b</sup> $P < 0.05$  compared with the respective SA-treated group by the fasting period. Seven rats were tested in each group. Open bars: SA-treated rats; closed bars: AG-treated rats.

*Figure 4. Effect of fasting and AG treatment on cell proliferation index in the jejunum.*

The jejunal crypt cell proliferation was histologically assessed by 5-BrdU incorporation to identify cells in the S phase of the cell cycle. The number of labeled cells in at least 10 well-oriented longitudinal crypts in each sample was determined and expressed as cell proliferation index (5-BrdU-positive cells/10 crypts). The decrease in cell proliferation along with fasting was observed both with and without AG. Values are means  $\pm$  SE. <sup>a</sup> $P < 0.05$  compared with the ad libitum-fed rats in SA-treated group. Seven rats were tested in each group. Open bars: SA-treated rats; closed bars: AG-treated rats.

*Figure 5. Effect of fasting and AG treatment on TUNEL staining and TUNEL-positive rate in the jejunal villus.*

Apoptotic assessment of the jejunal villus was performed using TUNEL staining and TUNEL-positive rate. A: TUNEL staining of representative jejunal section. TUNEL-positive cells were observed in the tip of the jejunal villus of SA-treated rats with increasing TUNEL-positive cells over the indicated fasting periods (A-1, A-2, C-1, C-2, E-1, E-2, G-1, G-2), which were all inhibited by AG (B-1, B-2, D-1, D-2, F-1, F-2, H-1, H-2). A-1, A-2: ad libitum-fed with SA treatment. B-1, B-2: ad libitum-fed with AG treatment. C-1, C-2: 24-h fasted with SA treatment. D-1, D-2: 24-h fasted with AG treatment. E-1, E-2: 48-h fasted with SA treatment. F-1, F-2: 48-h fasted with AG treatment. G-1, G-2: 72-h fasted with SA treatment. H-1, H-2: 72-h fasted with AG treatment. Magnification: left side  $\times 20$ , right side  $\times 80$ . B: The TUNEL-positive rate was determined by dividing the number of TUNEL-positive cells by the total number of cells in the villi and multiplying by 200. Fasting significantly induced jejunal cell apoptosis, which was completely inhibited by AG over the indicated fasting periods. Values are means  $\pm$  SE. <sup>a</sup>P < 0.05 compared with the ad libitum-fed rats in SA-treated group. <sup>b</sup>P < 0.05 compared with the respective SA-treated group by the fasting period. Seven rats were tested in each group. Open bars: SA-treated rats; closed bars: AG-treated rats.

*Figure 6. Effect of fasting and AG treatment on apoptotic index in the jejunal villus.*

The representative apoptotic changes by conventional light microscopy of HE-stained specimens (48-h fasted rat with SA treatment) are shown in Fig. 6A. The boxed areas (a, b, c) in

a low-power view of jejunal villi on the left ( $\times 20$ ) are seen at higher power on the right ( $\times 80$ ). Apoptotic cells in the villus are indicated by an arrow showing an intensely eosinophilic cytoplasm and nuclear fragmentation (a), condensed chromatin (b and c). Fig. 6B shows the AI in the villus of ad libitum and the indicated fasting periods (24 h, 48 h, 60 h, and 72 h) for SA treatment (top row) and AG treatment (bottom row). AI is defined as the total number of apoptotic cells at each cell position expressed as a percentage of the total number of cells counted at that cell position. Cell position 1 is defined as the cell at the crypt-villus junction. Seven rats were tested in each group.

*Figure 7. Effect of fasting and AG treatment on nitrite concentration in the jejunum.*

Jejunal nitrite concentrations were measured using HPLC. AG significantly inhibited the fasting-induced increase in the jejunal nitrite levels. Values are means  $\pm$  SE. <sup>a</sup>P < 0.05 compared with the ad libitum-fed rats in SA-treated group. <sup>b</sup>P < 0.05 compared with the respective SA-treated group by the fasting period. Seven rats were tested in each group. Open bars: SA-treated rats; closed bars: AG-treated rats.

*Figure 8. Effect of fasting and AG treatment on jejunal expression of iNOS mRNA.*

Levels of iNOS mRNA (101 bp) were assessed by densitometric analysis and are expressed as ratios of iNOS mRNA to GAPDH densitometry units. Fasting significantly induced iNOS

mRNA, which was suppressed by AG. Values are means  $\pm$  SE. <sup>a</sup>*P* < 0.05 compared with the ad libitum-fed rats in SA-treated group. Seven rats were tested in each group. Open bars: SA-treated rats; closed bars: AG-treated rats.

*Figure 9. Effect of fasting and AG treatment on jejunal expression of IFN- $\gamma$  mRNA.*

Levels of IFN- $\gamma$  mRNA (140 bp) were assessed by densitometric analysis and are expressed as ratios of IFN- $\gamma$  mRNA to GAPDH densitometry units. Fasting significantly induced IFN- $\gamma$  mRNA, which was suppressed by AG. Values are means  $\pm$  SE. <sup>a</sup>*P* < 0.05 compared with the ad libitum-fed rats in SA-treated group. Seven rats were tested in each group. Open bars: SA-treated rats; closed bars: AG-treated rats.

*Figure 10. Light micrographs of the jejunum immunohistochemically stained for iNOS.*

Negligible iNOS staining was noted in the crypts and only faint staining in the cytoplasm at the villus-tip epithelial cells of ad libitum-fed rats (A-1 and A-2). Decrease of these stainings with AG treatment in ad libitum-fed rats (B-1 and B-2). Fasting for 24 h, 48 h, and 72 h revealed heavily positive iNOS immunostaining along the mucosal epithelial monolayer of the jejunum (C-1, C-2; E-1, E-2; and G-1, G-2). These enhanced iNOS immunoreactivities were almost completely inhibited by AG treatment (D-1, D-2; F-1, F-2; and H-1, H-2). A-1, A-2: ad libitum-fed with SA treatment. B-1, B-2: ad libitum-fed with AG treatment. C-1, C-2: 24-h

fasted with SA treatment. D-1, D-2: 24-h fasted with AG treatment. E-1, E-2: 48-h fasted with SA treatment. F-1, F-2: 48-h fasted with AG treatment. G-1, G-2: 72-h fasted with SA treatment. H-1, H-2: 72-h fasted with AG treatment. Magnification: left side  $\times 20$ , right side  $\times 80$ .

*Figure 11. Effect of fasting on jejunal expression of nNOS mRNA.*

Levels of nNOS mRNA (146 bp) were assessed by densitometric analysis and are expressed as ratios of nNOS mRNA to GAPDH densitometry units. In contrast to iNOS (Fig. 7), fasting significantly attenuated nNOS mRNA levels. Values are means  $\pm$  SE. <sup>a</sup>P < 0.05 compared with the ad libitum-fed rats in SA-treated group. Seven rats were tested in each group.

*Figure 12. Effect of fasting and AG treatment on DNA oxidative damage in the jejunum.*

DNA oxidative damage was assessed by levels of 8-OHdG in the jejunum. In SA-treated groups, fasting increased jejunal 8-OHdG levels at 24 h, 48 h, and 72 h fasting periods compared with the ad libitum-fed rats. AG significantly inhibited the fasting-induced increases in the jejunal 8-OHdG levels at 48 h and 72 h fasting periods compared with the respective SA-treated group at each fasting period. <sup>a</sup>P < 0.05 compared with the ad libitum-fed rats in SA-treated group. <sup>b</sup>P < 0.05 compared with the respective SA-treated group at each fasting period. Seven rats were tested in each group. Open bars: SA-treated rats; closed bars: AG-treated rats.

*Figure 13. Schematic summary diagram of fasting-induced intestinal apoptosis.*

This schematic summary diagram depicts a possible role of nNOS in the regulation of iNOS activity upstream in the process of fasting-induced apoptosis. iNOS-derived NO may play a central role downstream in this process, inducing IFN- $\gamma$ , and leading to IEC apoptosis. Note a close interaction between iNOS-released NO in IEC and IEL-derived IFN- $\gamma$  through a ROS-mediated mechanism in the intestinal mucosa. IEC: intestinal epithelial cell, IEL: intraepithelial lymphocyte.

*Table 1. Enterocyte apoptosis of the jejunal villus by conventional light microscopy of HE-stained specimens.*

Significant decreases in cell numbers per villus column of fasting rats were noted compared to that of the ad libitum-fed rats over the indicated time periods. Conventional light microscopy detecting representative apoptotic changes showed significant increases both in ratio of apoptotic cells to one villus column and in AI (6.8- to 8.6-fold increase:  $P < 0.05$ ) in fasted rats with SA, and also showed significant inhibitory effects of AG on fasting-induced apoptosis over the indicated fasting periods. Values are means  $\pm$  SE;  $n = 7$  per group. <sup>a</sup> $P < 0.05$  compared with the ad libitum-fed rats in SA-treated group. <sup>b</sup> $P < 0.05$  compared with the respective SA-treated group at each fasting period. AI in the villus is defined as the total number of apoptotic cells expressed as a percentage of the total number of cells counted in 50 well-oriented villus columns.

AI: apoptotic index

Fig. 1

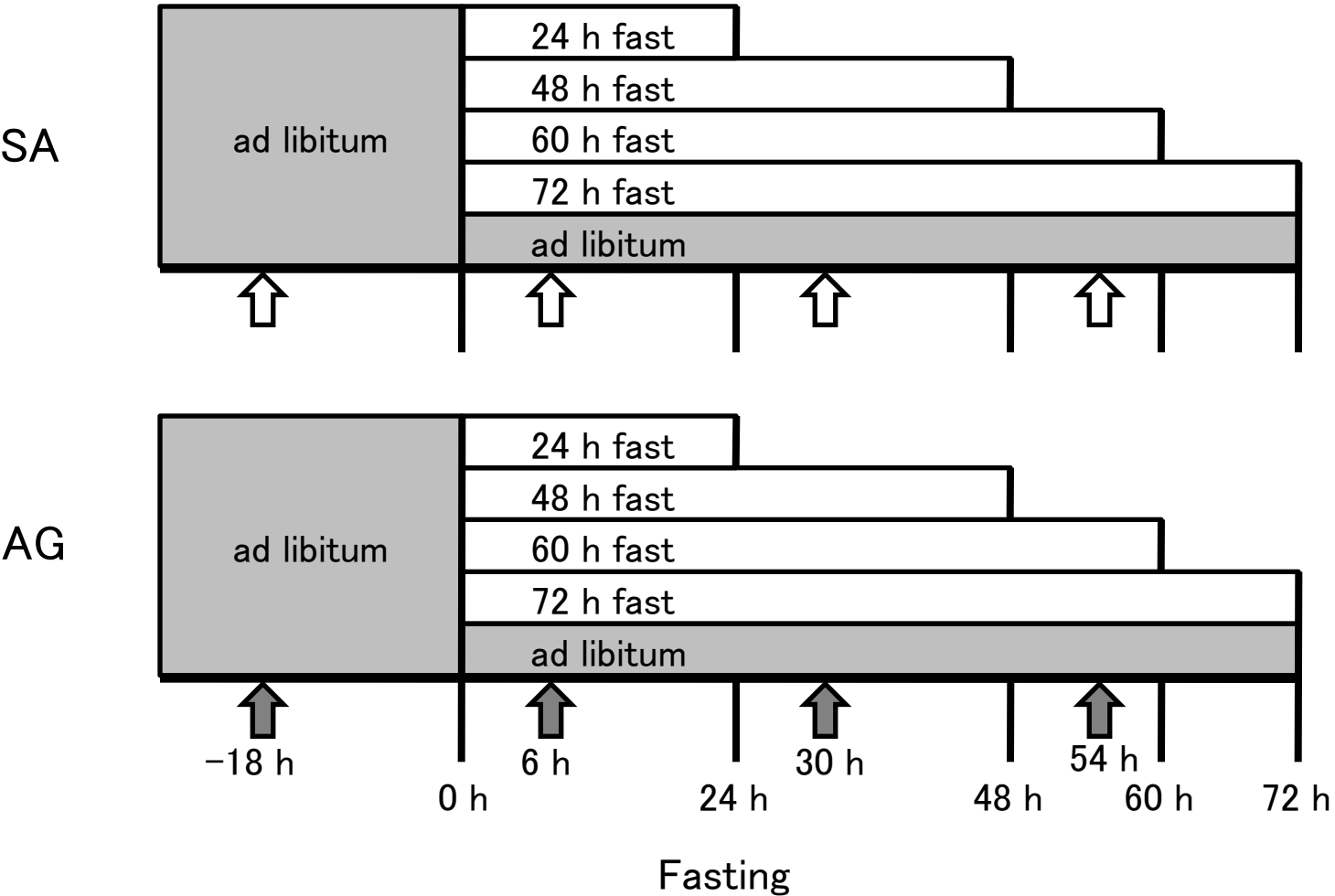


Fig. 2

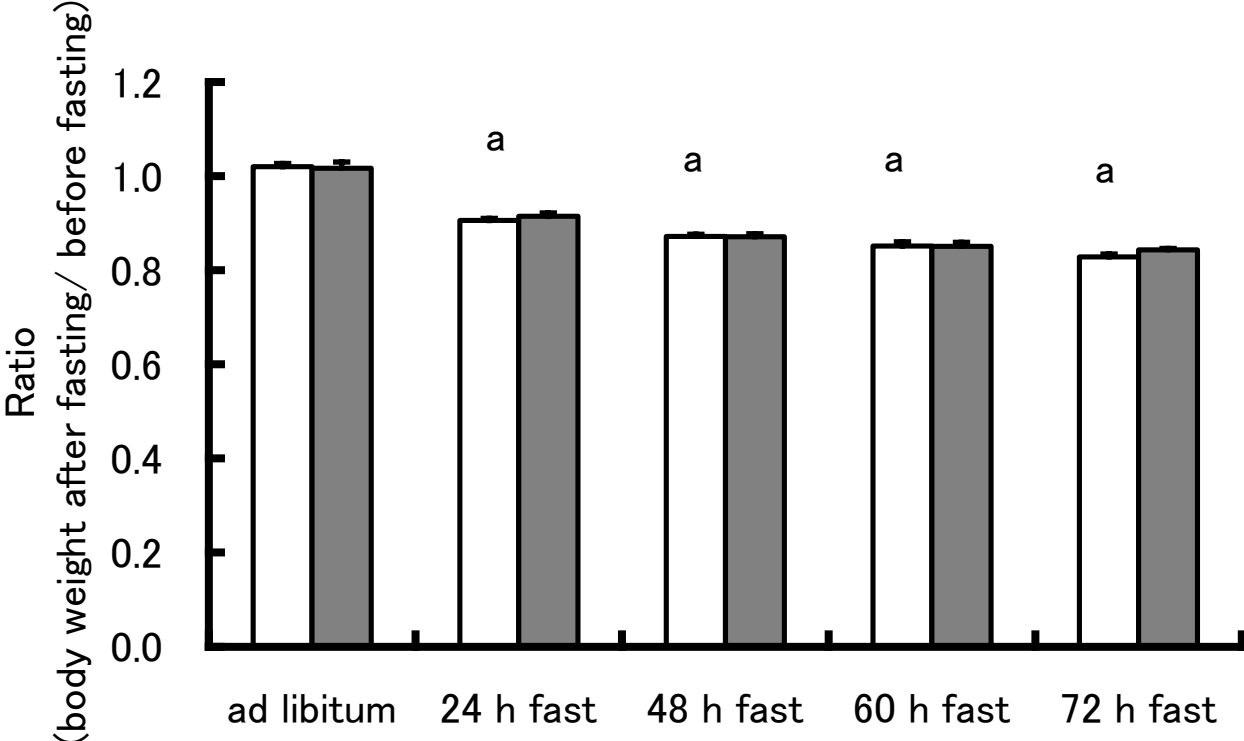


Fig. 3

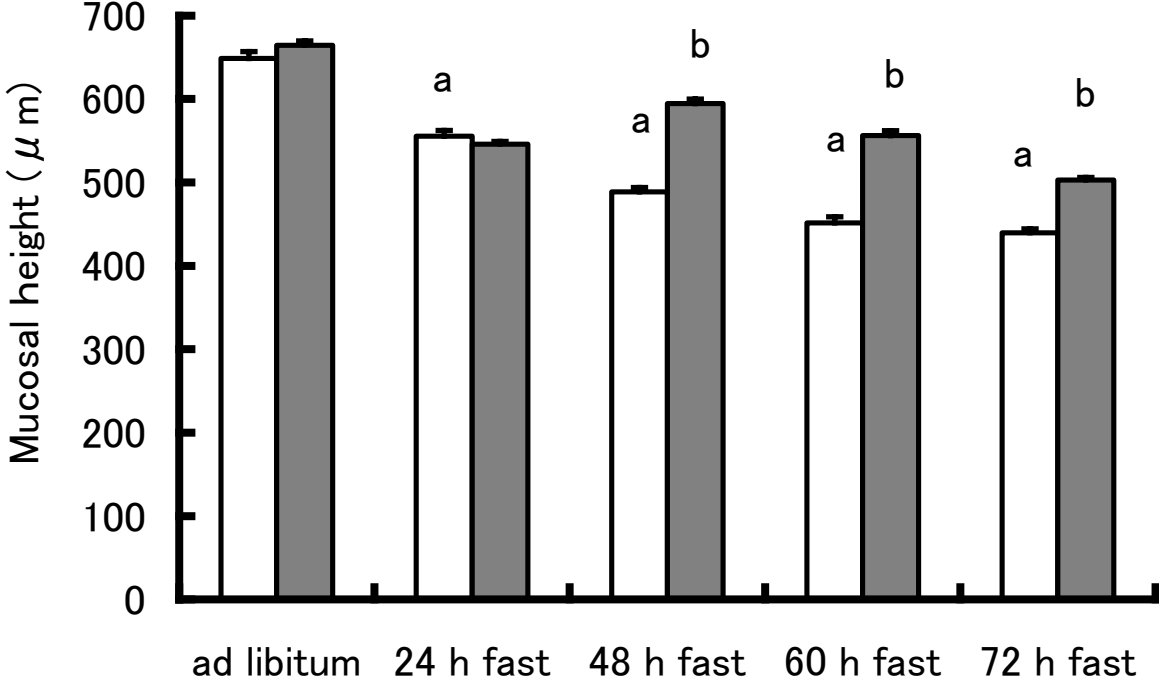


Fig. 4

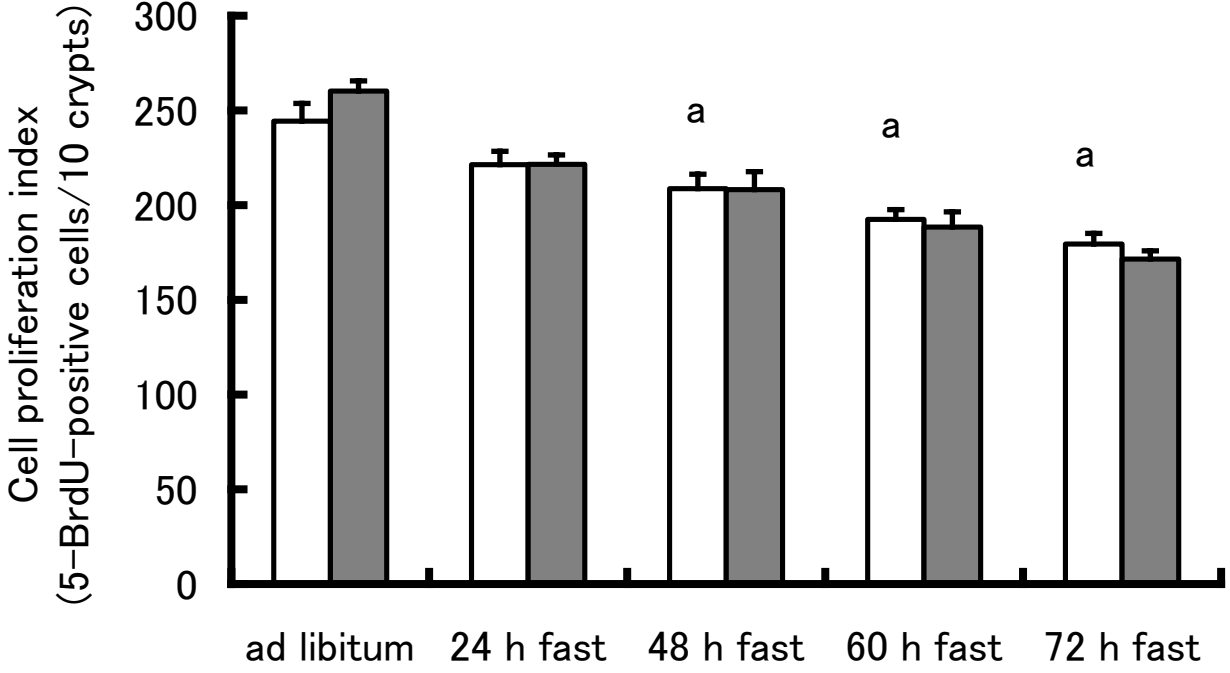


Fig. 5 A

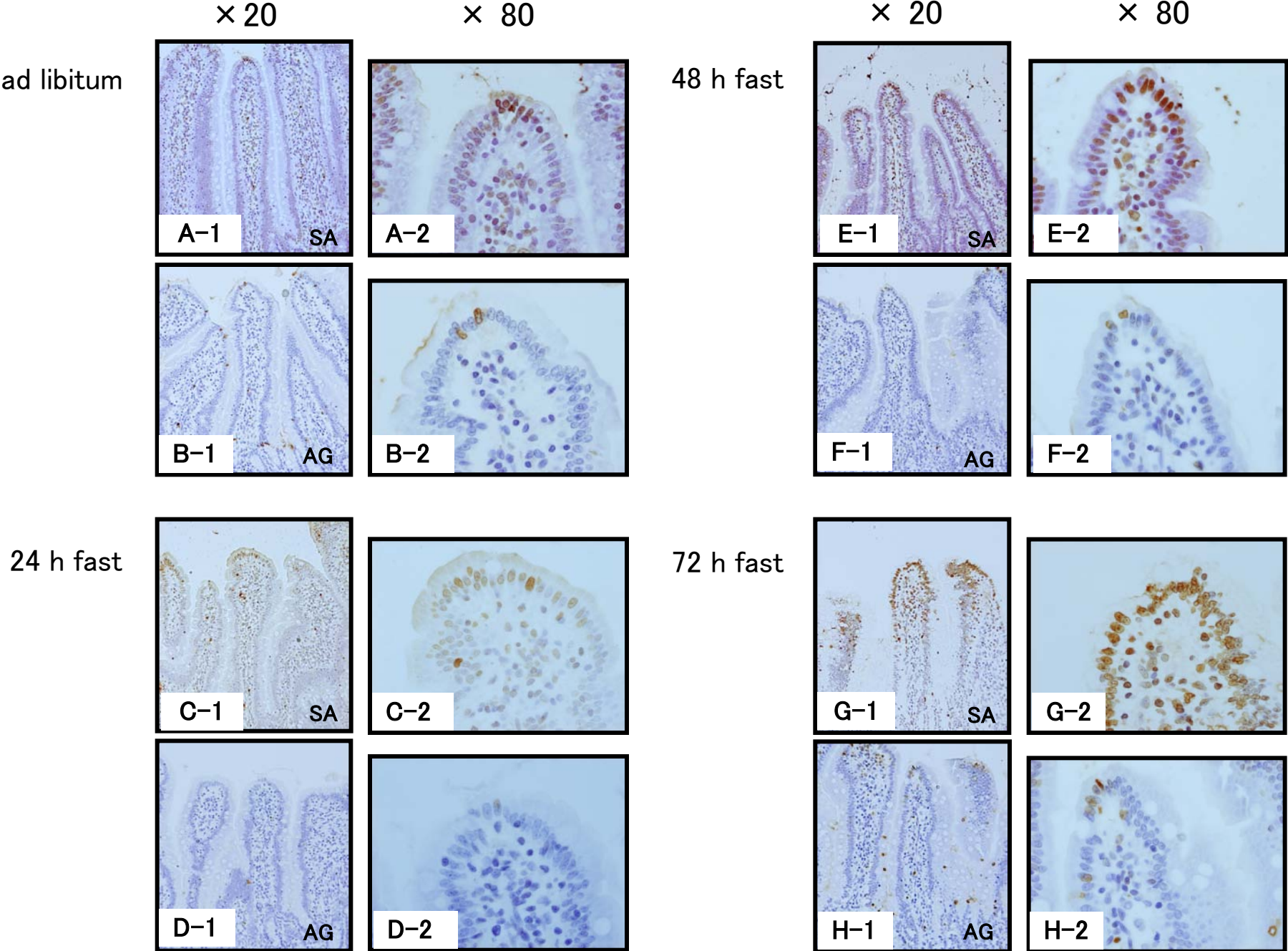


Fig. 5 B

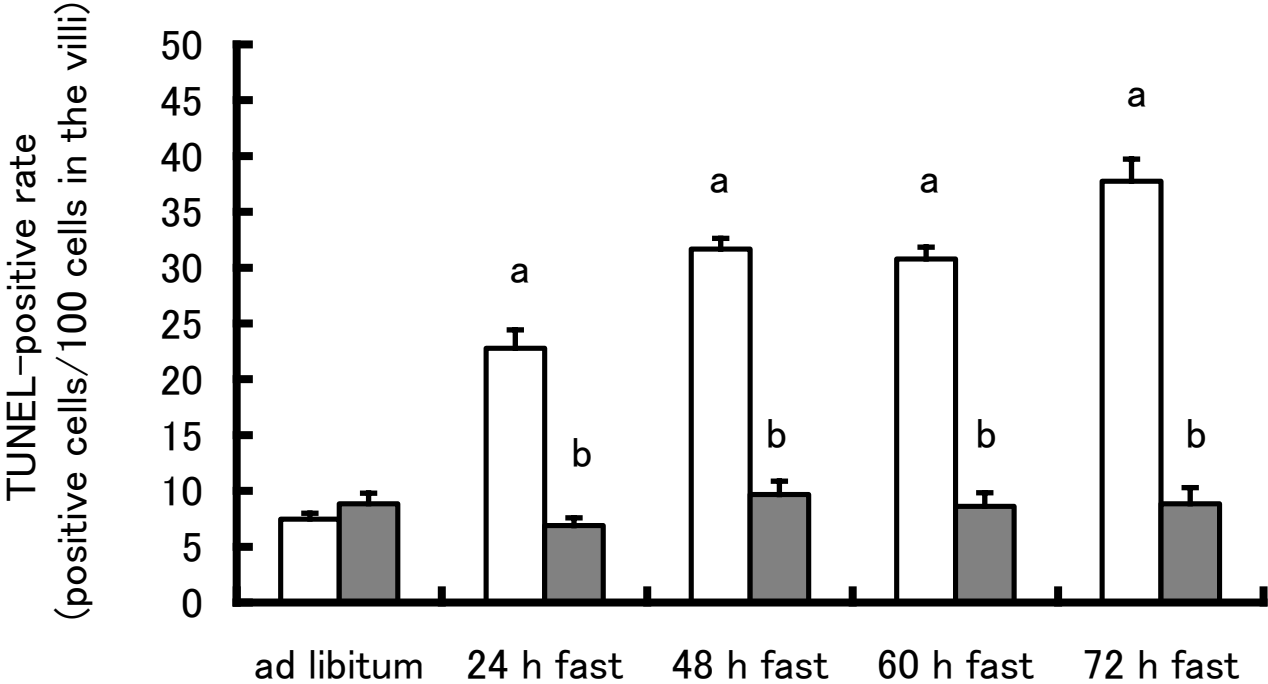


Fig. 6 A

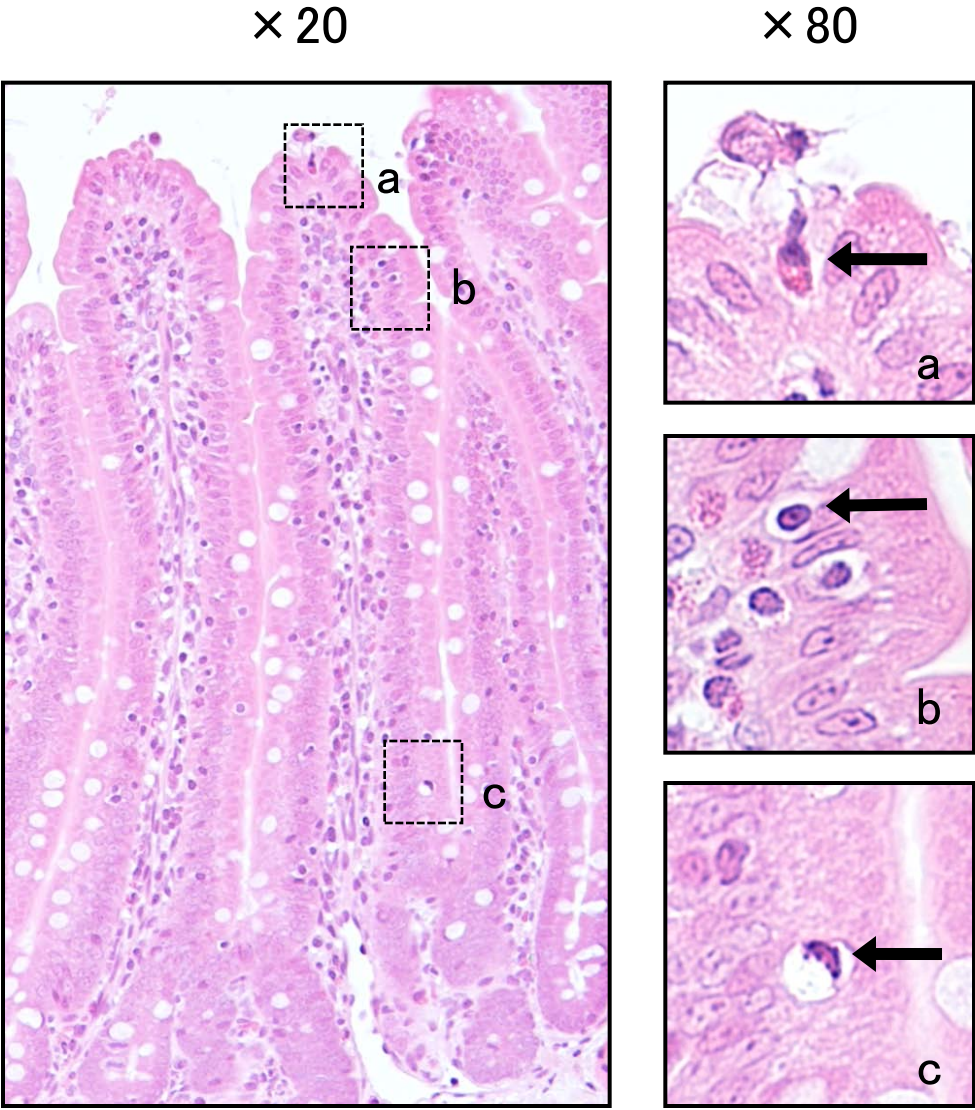
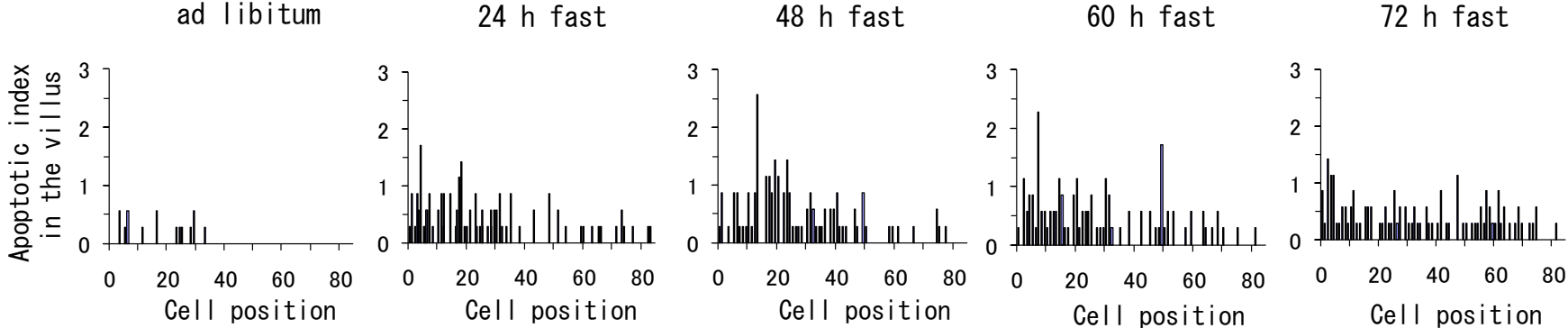


Fig. 6 B

SA



AG

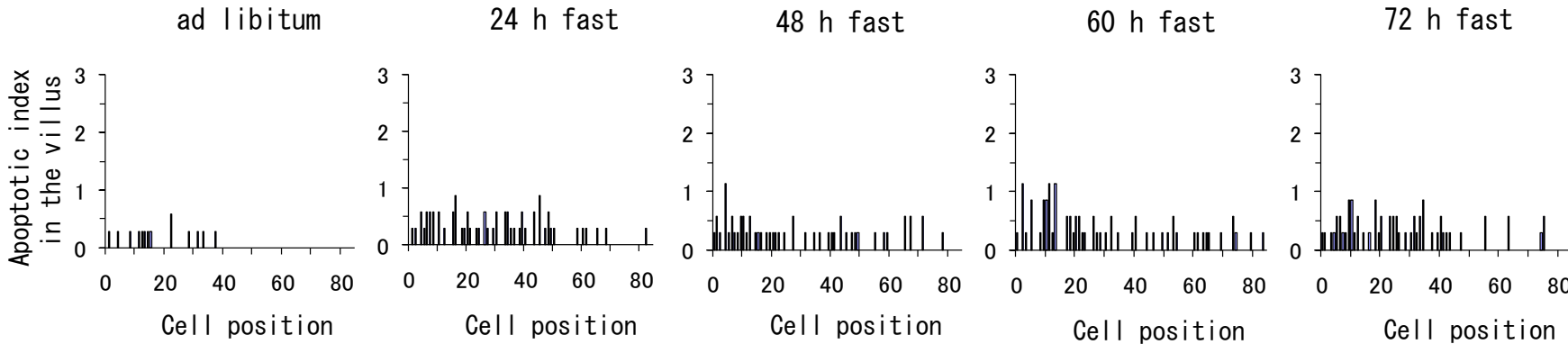


Fig. 7

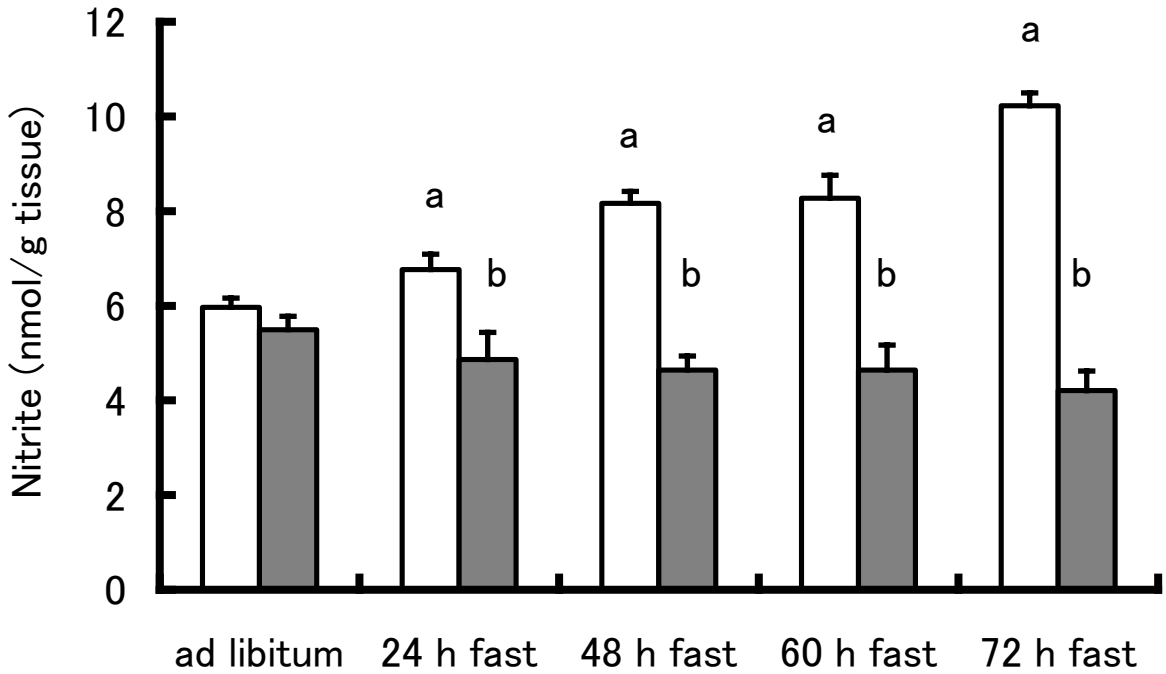


Fig. 8

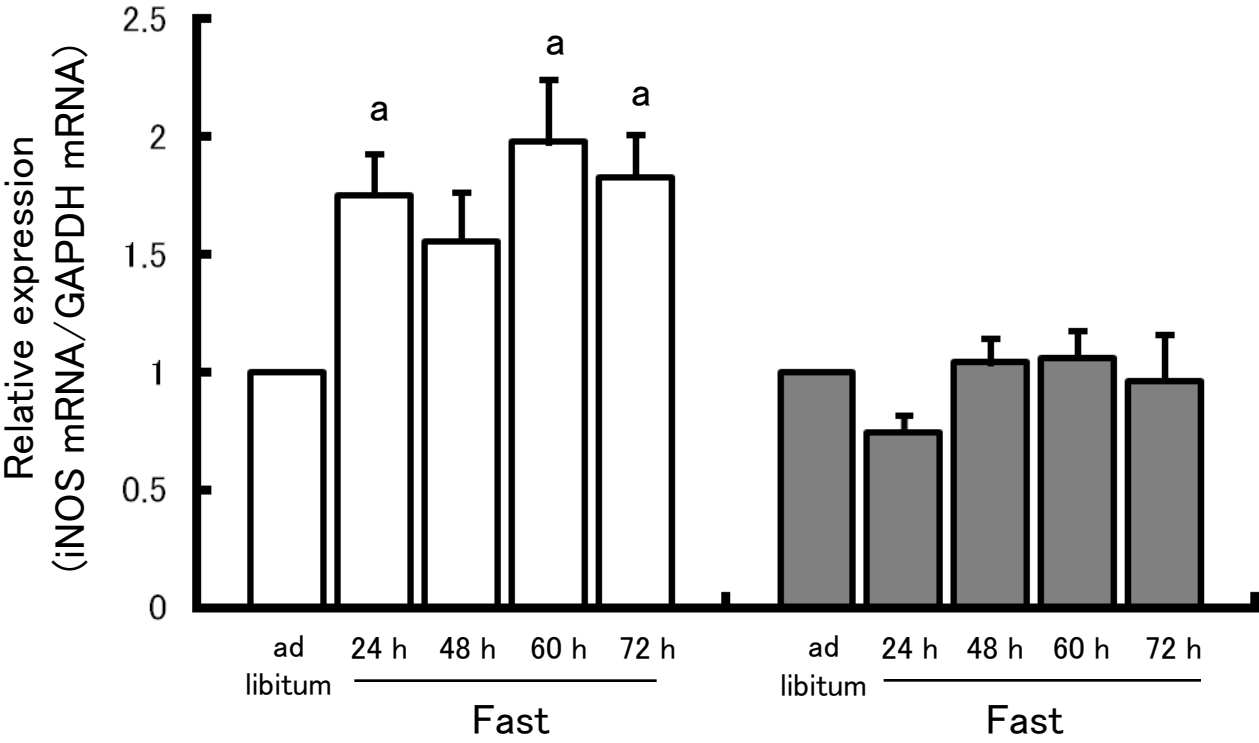
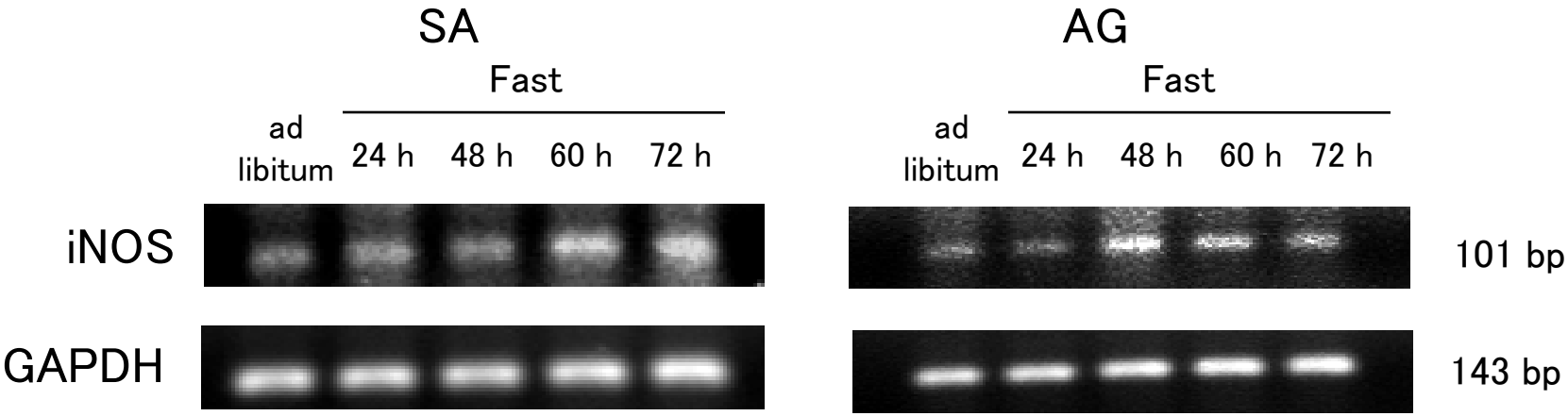


Fig. 9

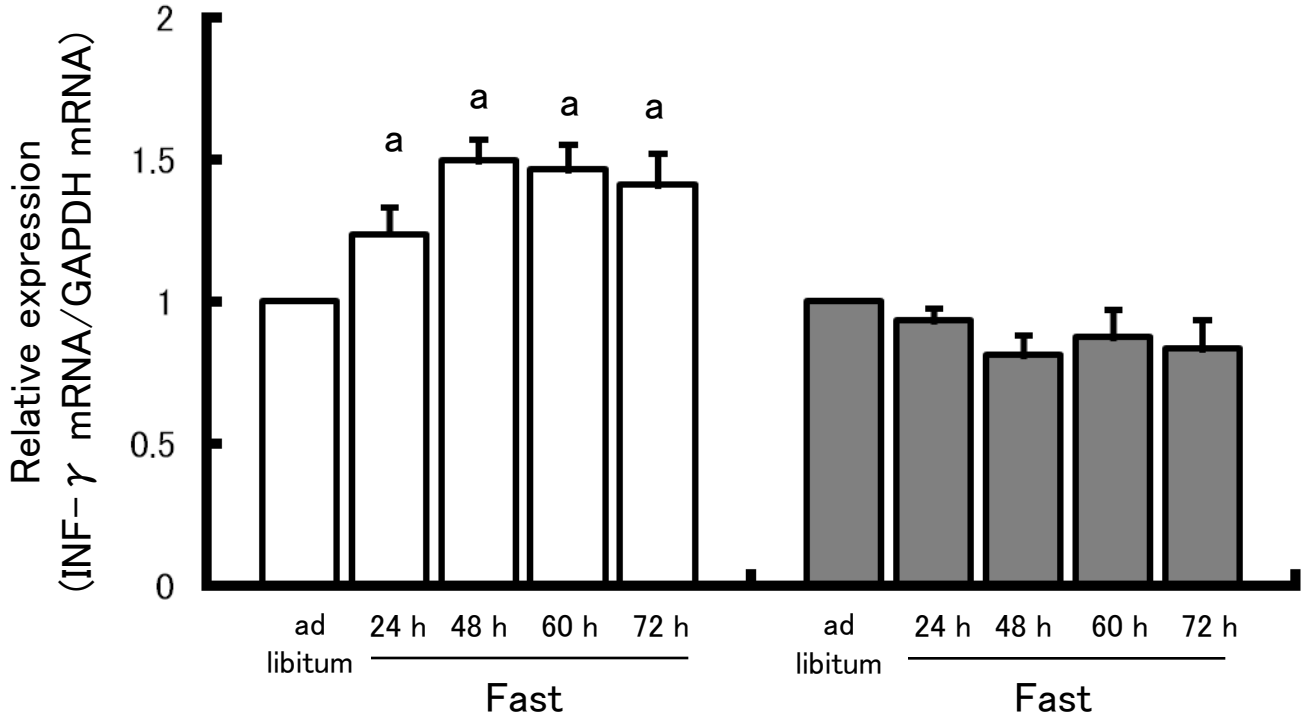
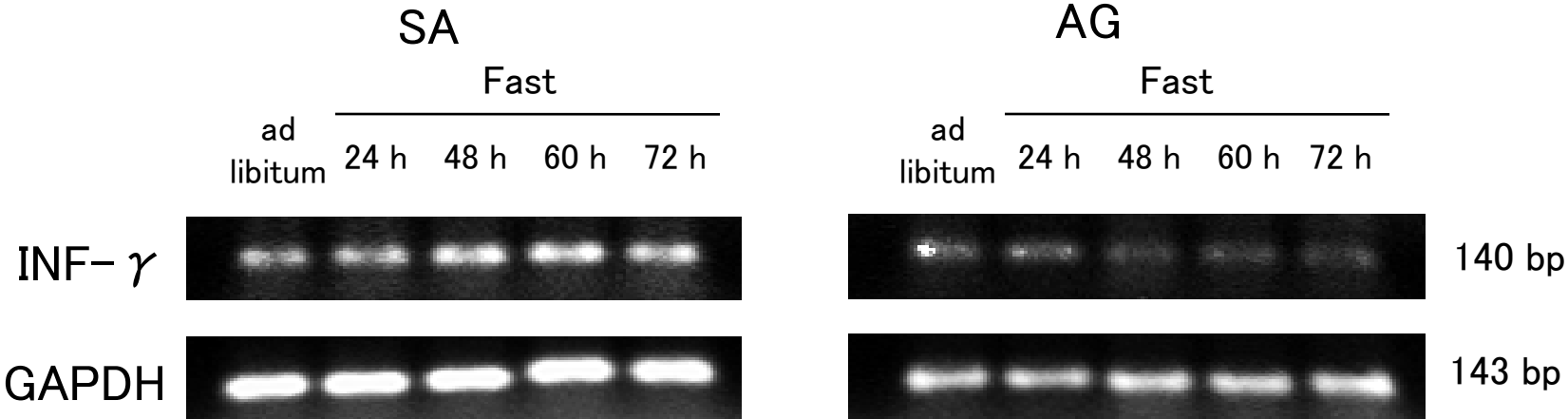


Fig. 10

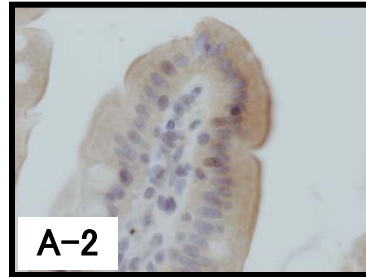
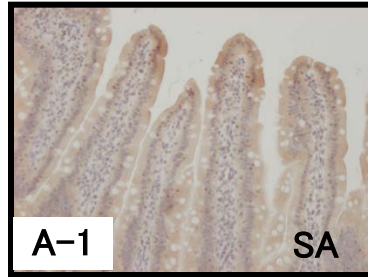
× 20

× 80

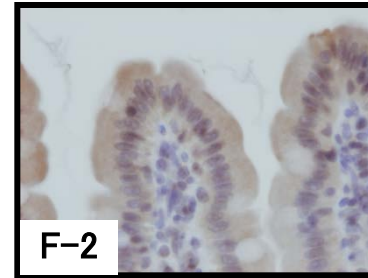
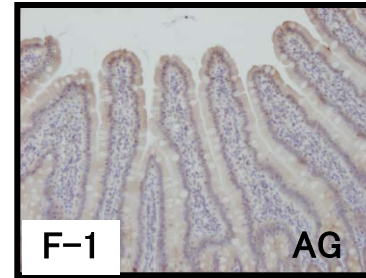
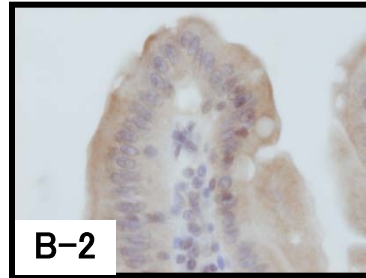
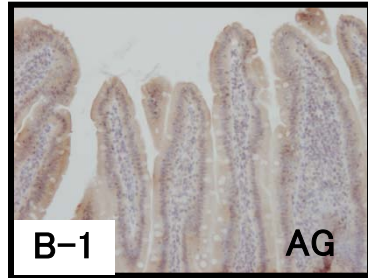
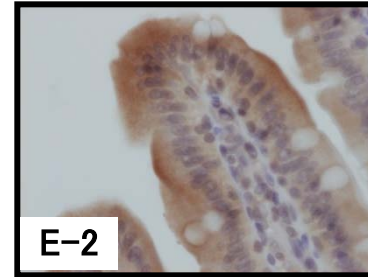
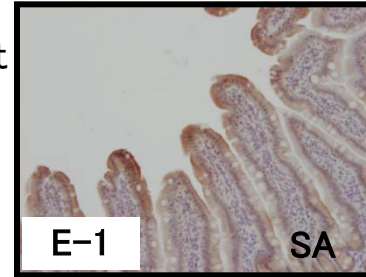
× 20

× 80

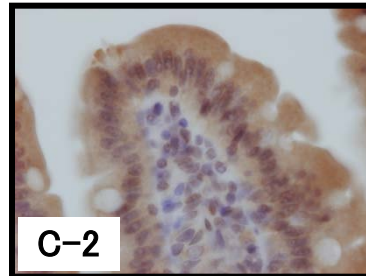
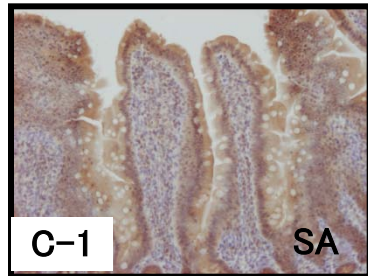
ad libitum



48 h fast



24 h fast



72 h fast

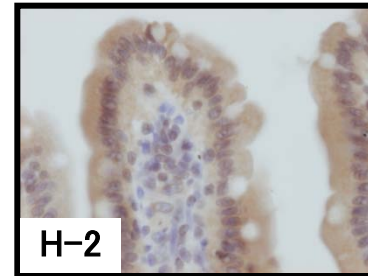
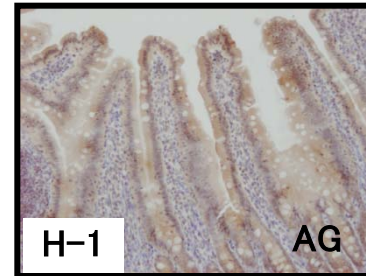
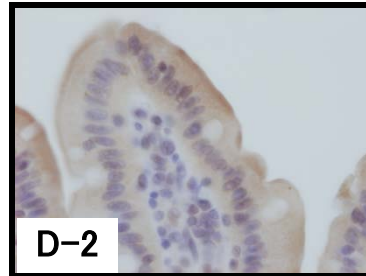
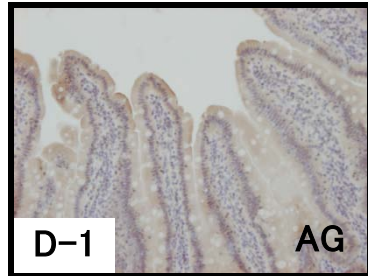
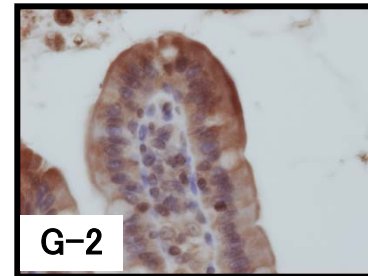
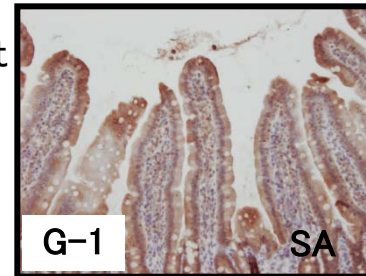


Fig. 11

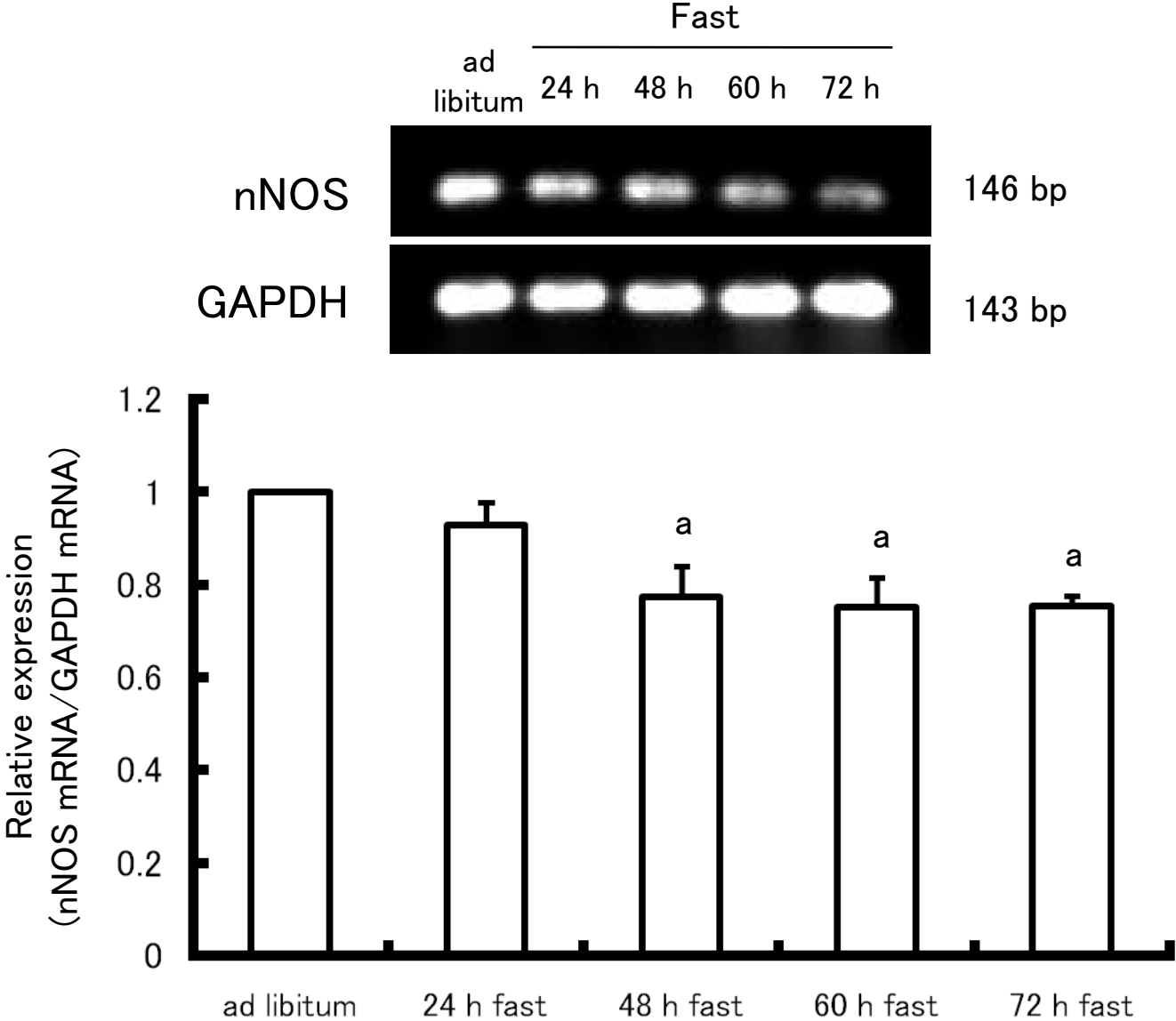


Fig. 12

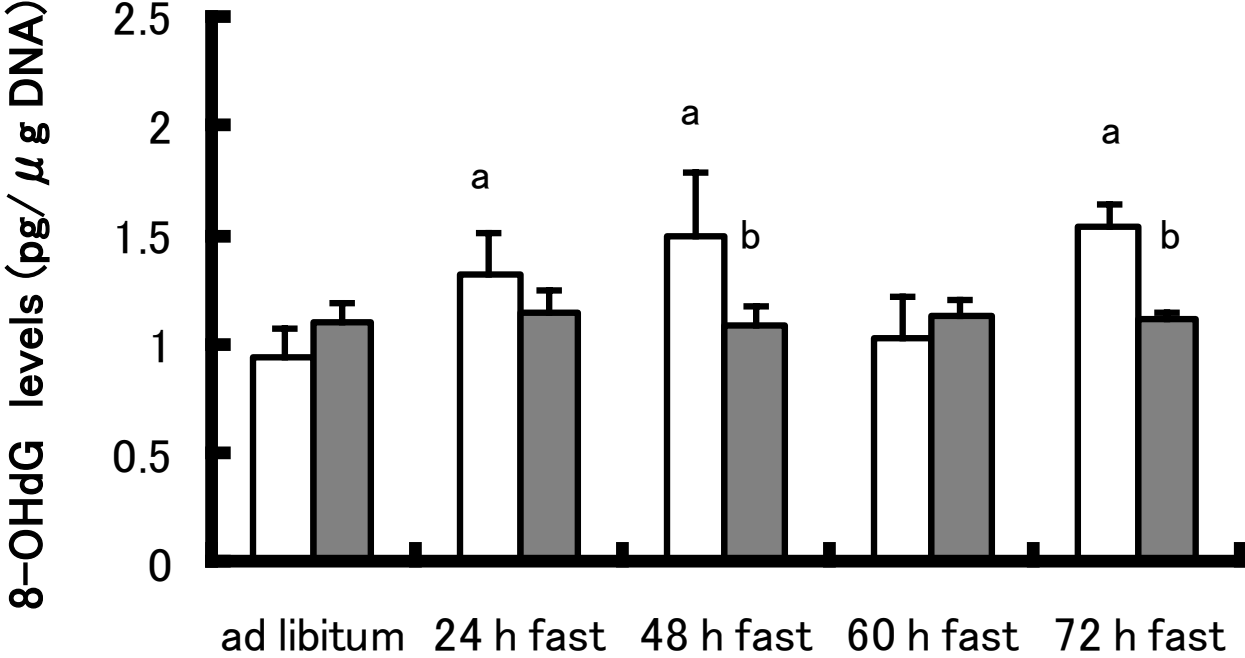


Fig. 13

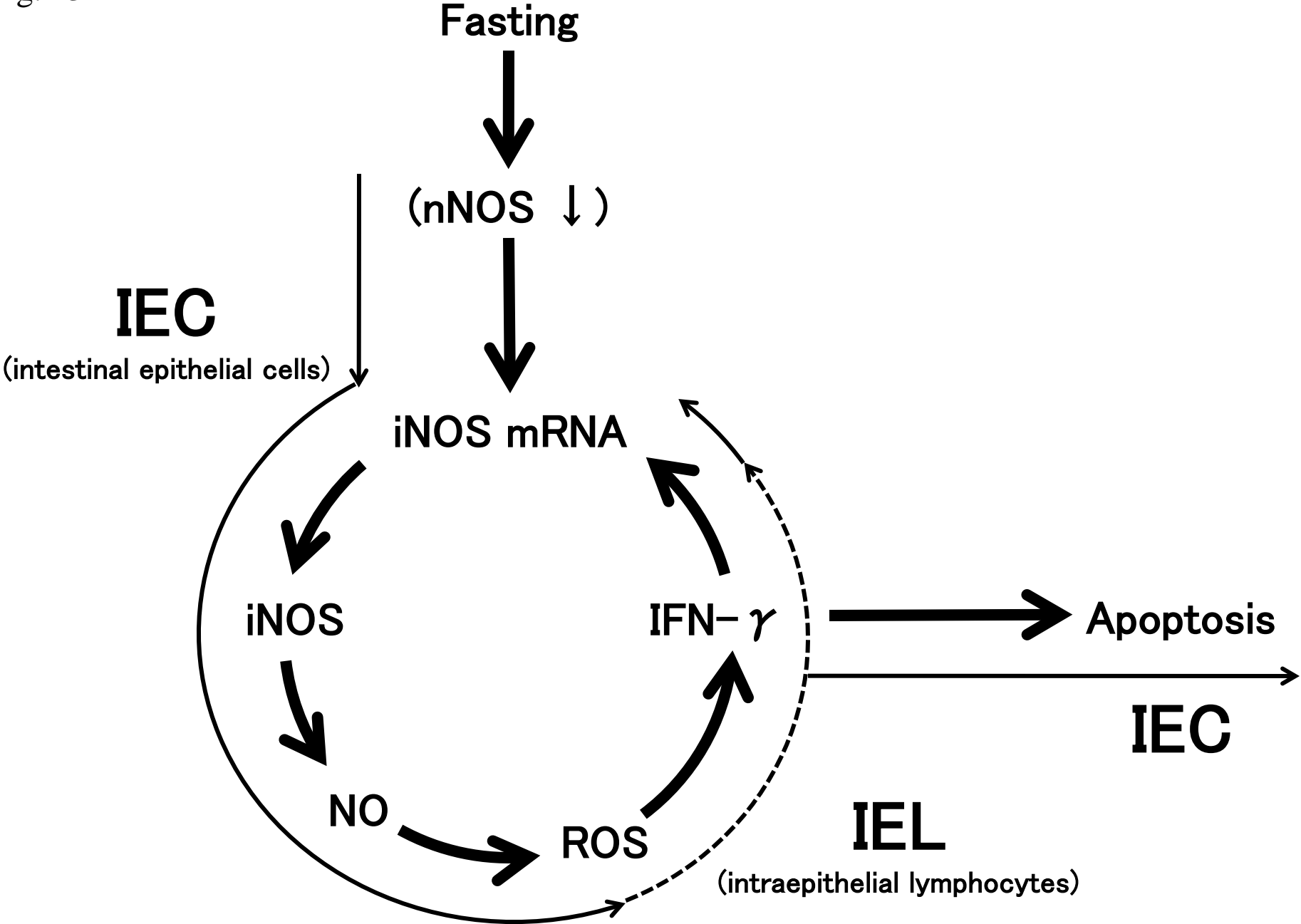


Table. 1

	ad libitum	24 h fast	48 h fast	60 h fast	72 h fast
SA					
Cells per villus column, n	84 ± 1	72 ± 1 <sup>a</sup>	70 ± 2 <sup>a</sup>	70 ± 2 <sup>a</sup>	68 ± 1 <sup>a</sup>
Apoptotic cells per villus column, n	0.04 ± 0.01	0.24 ± 0.04 <sup>a</sup>	0.29 ± 0.02 <sup>a</sup>	0.29 ± 0.02 <sup>a</sup>	0.29 ± 0.04 <sup>a</sup>
Apoptotic index, %	0.05 ± 0.01	0.34 ± 0.07 <sup>a</sup>	0.42 ± 0.03 <sup>a</sup>	0.42 ± 0.02 <sup>a</sup>	0.43 ± 0.05 <sup>a</sup>
AG					
Cells per villus column, n	85 ± 1	75 ± 1	76 ± 3	75 ± 1	75 ± 2
Apoptotic cells per villus column, n	0.04 ± 0.01	0.17 ± 0.02 <sup>b</sup>	0.15 ± 0.01 <sup>b</sup>	0.19 ± 0.03 <sup>b</sup>	0.17 ± 0.03 <sup>b</sup>
Apoptotic index, %	0.05 ± 0.01	0.22 ± 0.02 <sup>b</sup>	0.20 ± 0.02 <sup>b</sup>	0.25 ± 0.04 <sup>b</sup>	0.23 ± 0.04 <sup>b</sup>